

# Planet Migration

To Appear in "Exoplanets," ed. S. Seager, Univ. Arizona Press.

**Stephen H. Lubow**

Space Telescope Science Institute

**Shigeru Ida**

Tokyo Institute of Technology

Planet migration is the process by which a planet's orbital radius changes in time. The main agent for causing gas giant planet migration is the gravitational interaction of the young planet with the gaseous disk from which it forms. We describe the migration rates resulting from these interactions based on a simple model for disk properties. These migration rates are higher than is reasonable for planet survival. We discuss some proposed models for which the migration rates are lower. There are major uncertainties in migration rates due to a lack of knowledge about the detailed physical properties of disks. We also describe some additional forms of migration.

## 1. INTRODUCTION

Planet formation occurs in disks of material that orbit young stars (see Chapter 13). At early stages of evolution, the disks are largely gaseous and have masses of typically a few percent or more of the stellar masses. At later times, after several  $10^6$  yr, the gas disperses and disks largely consist of solid material. Such disks last for timescales of  $\sim 10^8$  yr. The interactions of a young planet with its surrounding disk affects the planet's orbital energy and angular momentum. One consequence of such interactions is that a planet may move radially through the disk (toward or away from the central star), a process called migration that is the topic of this chapter. In this chapter, we mainly concentrate on migration caused by gaseous disks. Although gaseous disks survive only a small fraction of the lifetime of the star and planet ( $\sim 10^{10}$  yr), calculations of disk-planet interactions described in this chapter show them to be strong enough to have caused substantial migration. In fact, a major problem is that the effects of migration are typically predicted to be too strong to have allowed the formation of gas giant planets to complete. That is, the typical timescales for migration are found to be shorter than both the lifetimes of gaseous disks and the predicted formation timescales of gas giant planets in the so-called core accretion model of  $\sim 10^6$  yr (see Chapter 13). Migration models applied some simple disk structures predict that a forming planet should fall into (or very close to) the central star before it grows in mass to become a gas giant (Ward, 1997).

Early theoretical studies of planet migration, such as Goldreich & Tremaine, 1980, understandably concentrated on the role of migration for the planets in our solar system. These studies suggested that there was substantial migration of Jupiter while it was immersed in the solar nebula. Migration should have occurred both at Jupiter's early stages of

formation when it was a solid core and at later stages when it was a fully developed gas giant planet interacting with the solar nebula. The migration timescales were estimated to be much shorter than lifetime of the nebula, although the direction of migration was not determined. However, the evidence for migration was not apparent. The location of Jupiter is just outside the snow-line, where conditions for rapid core formation are most favorable (see Chapter 13). This situation seemed to suggest that Jupiter formed and remained near its current location. Therefore, a plausible conclusion was that migration did not play an important role for Jupiter and therefore perhaps for all planets.

Evidence for the importance of migration changed dramatically in 1995 with the discovery of the first giant planet, 51 Peg b, that has an orbital period of only about 4 days (Mayor and Queloz, 1995). Subsequent discoveries of many giant planets with orbital radii substantially smaller than Jupiter's added to the evidence (e.g., Butler et al, 2006). Their existence suggested that migration had occurred, since giant planet formation close to a star is not likely to occur (Bodenheimer et al, 2000; Ida & Lin, 2004).

We might crudely think of a planet orbiting in a gaseous disk around a star as being similar to a satellite in orbit about the Earth. Atmospheric gas drag on the satellite causes it to lose angular momentum and spiral down (migrate inwards) towards the Earth. However, the disk-planet situation is somewhat different. The planet and disk are both in orbit about the star, and there is a relatively small difference between the rotational speeds of the planet and its neighboring gas. Although the velocity difference can produce an important level of gas drag for small mass solid objects, gas drag does not produce the dominant torque for objects as large as planets, as is discussed further in Section 2.1. For disk-planet interactions, gravitational torques play the dominant role.

The gravitational interactions between a planet and a gaseous disk are difficult to analyze in a precise way. But a general picture has developed. The results depend somewhat on the disk structure. We consider the disk to be what is called an accretion disk. Accretion disks occur in many astronomical objects, such as binary star systems and active galactic nuclei. Such disks typically arise as gas flows towards a central body with some rotation about that body. Due to its angular momentum, the gas cannot fall directly onto the central object and instead forms a disk in near centrifugal balance. Observations of such systems, including disks around young stars, reveal evidence that the gas is not simply orbiting about the star, but also flowing inward (accreting) towards the central object. The inflow velocity within the disk is very small compared to the orbital velocity. But it is sufficient to reveal various observational signatures as a consequence of this mass flow towards and onto the central object. In particular, the inflow can result in the emission of radiation from the accreting gas as it moves deeper in the gravitational potential of the central object. In the case of interest to planet migration, the gaseous disk orbits about a young central star. These so-called protoplanetary disks are described in Chapter 11.

Turbulence within the disk is thought to be the main driver of the accretion. The disk does not rotate about the star at a constant rate with distance from the star. Instead, as a consequence of centrifugal balance, it undergoes differential rotation, and the gas rotation rate decreases with distance from the star. The gas orbits at (nearly) the so-called Keplerian orbital frequency at orbital radius  $r$  from the star of mass  $M_s$  given by

$$\Omega(r) = \sqrt{\frac{GM_s}{r^3}}. \quad (1)$$

In a simple model, the disk turbulence can be considered to cause an effective friction. Neighboring rings of gas in the disk interact by frictional forces as they rub against each other due to the differential rotation. This friction produces orbital energy losses and a torque that causes nearly all the material within the disk to move in (accrete), while angular momentum is transported outward (*Lynden-Bell & Pringle, 1974*). Instabilities within the disk are the cause of the turbulence. The most likely candidates for causing the instabilities are disk self-gravity (e.g., *Paczynski, 1978*; *Lodato & Rice, 2004*) and magnetic fields (*Balbus & Hawley, 1991*). Disk self-gravity instabilities are more likely to be important at the earliest stages of disk evolution, while it is more massive.

For small mass planets, the density structure of the disk is largely unaffected by the presence of the planet. This situation leads to the so-called Type I regime of planet migration. In this simple model, the disk density structure is determined by the disk turbulence. The disk differential rotation implies that gas that lies outside the orbit of the planet moves more slowly than gas inside the orbit of the planet. The planet disturbs the disk by its gravity as gas passes near it. The disk disturbances act back on the planet and cause

a net torque to be exerted on the planet. This torque causes the planet to migrate. An analysis, such as in Section 2.2, shows that the migration timescale (orbit decay timescale) for a 10 Earth mass planet embedded in a disk that is somewhat similar to the minimum mass solar nebula (*Hayashi, 1981*) is only about  $10^5 y$  (see Fig. 1). Furthermore, the migration timescale varies inversely with planet mass. This result has the consequence that planets migrate even faster as they grow in mass. The shortness of this timescale poses a challenge to our understanding of migration, as discussed earlier.

For a sufficiently high mass planet, its tidal torques can overpower the viscous torques associated with disk turbulence, and the planet can alter the disk density in its vicinity. The result is that the planet opens a gap in the disk about its orbit. In this situation, we have the so-called Type II regime of planet migration. The disk-planet interactions in this case are still gravitational. But the gravitational torque on the planet is reduced because there is less material close to the planet compared to the Type I regime. In the limiting case that the planet mass is small compared to the disk mass, the planet moves inward like a test particle along with the accretion inflow of the gas. The disk, being much more massive than the planet, sets the migration rate of the planet to its inflow rate. The disk density near the gap region adjusts so that the torque on the planet matches the disk's inflow speed.

The mass required for the planet to open a gap, as well as the migration rate, depends on the level of disk turbulence. For typically adopted disk parameters, the transition to Type II migration occurs at a few tenths of a Jupiter mass. The migration timescales are about  $10^5 \text{yr}$ . This timescale is also short compared to the disk lifetimes, but is much longer than it would have been if the planet had continued to undergo Type I migration (see Fig. 1). In this idealized Type II regime of high disk-to-planet mass ratio, the planet migration rate is independent of planet mass, since it is determined by the disk only. But for less extreme disk-to-planet mass ratios, the inertia of the planet plays a role and the migration rate decreases somewhat with planet mass.

The determination of planet migration rates is not easy and various aspects remain controversial. There are several reasons for this. Although the interaction between a planet and its surrounding disk is gravitational, the interaction behaves in a way that is reminiscent of friction (dynamical friction). Gas that lies somewhat exterior (interior) to the planet's orbit rotates slower (faster) than the planet and provides an inward (outward) torque on the planet as a consequence of the interaction. The net torque therefore involves a competition between nearly equal and opposite torques. Accurate calculations of the inward and outward torques are then required to determine the migration rate and the direction of migration. Another complication is that the disk-planet interactions generally get stronger closer to the planet. The results therefore depend on the details of how these torques become limited near the planet.

Another issue involves the effects of material that lies

very close to the planet. This so-called coorbital region involves gas that does not circulate past the planet (see Fig. 2). Instead, the gas undergoes abrupt changes in its angular momentum due to encounters with the planet that take it from interior of the planet’s orbit radius to exterior of the planet’s orbital radius and visa-versa. The torques resulting from this region are quite different from those involving more weakly perturbed material that lies outside this region. The two regions, the weakly deflected and strongly deflected regions, are dynamically quite different and require separate descriptions. Yet another issue is that the torques depend on the detailed conditions within the disk. The disk structural variations, i.e., how the disk density and temperature vary in radius, can play an important role in determining the torque. The detailed structural properties of disks around young stars are not well understood and could be complicated (e.g., *Armitage et al*, 2000; *Terquem*, 2008). The resulting structures are likely more complicated than the simple power-law density distributions of the minimum mass solar nebula model. The level of disk turbulence in a protostellar disk influences the disk structure and the rate of planet migration. The amount turbulence can vary with distance from the star and in time, but it is not well understood.

In Section 2 we describe calculations of migration rates due to disk-planet interactions. Section 2.1 discusses the effects of gas drag. Section 2.2 describes the migration rate of a low mass planet interacting with a disk, modeled simply as a set of ballistic particles that undergo mild or weak interactions with the planet. This leads to an estimate of the migration rate, but the approximations are not accurate enough to determine the direction of migration. Sections 2.3 discusses the torques due to material that comes very close to the planet, torques in the coorbital region. Section 2.4 discusses the more accurate determination of Type I migration rates for a gaseous disk and the factors affecting migration. Section 3 describes some of the outstanding issues: how planet migration may be slower than estimated in Section 2, some effects in planet migration that are missing from the idealized models in Section 2, some forms of migration not involving a gaseous disk, and some issues about the techniques used in carrying out numerical simulations. Section 4 describes some future prospects.

## 2. Migration Rates Due To Disk-Planet Interactions

### 2.1 Aerodynamic Gas Drag

Aerodynamic gas drag provides the dominant influence on the orbital evolution of low mass solids embedded in a gaseous disk that orbits a star (*Weidenschilling*, 1977; *Cuzzi & Weidenschilling*, 2006). The gas is subject to a radial pressure force, in addition to the gravitational force of the star. For a disk with smooth structural variations in radius, this force induces slight departures from Keplerian speeds of order  $(H/r)^2\Omega r$ , where  $H$  is the disk thickness and  $\Omega$  is the angular speed of the disk at radius  $r$  from the star. For a thin disk ( $H \ll r$ ) whose pressure declines in radius, as is

typically expected, the pressure force acts radially outward. The gas rotation rate required to achieve centrifugal balance is then slightly below the Keplerian rate. Sufficiently high mass solids are largely dynamically decoupled from the gas and orbit at nearly the Keplerian rate, but are subject to drag forces from the more slowly rotating gas. The drag leads to their orbit decay. Both the drag force and the inertia increase with the size of the solid,  $R$ . The drag force on the object increases with its area ( $\sim R^2$ ), while its inertia increases with its volume ( $\sim R^3$ ). In the high mass solid regime, the dominance of inertia over drag causes the orbital decay rate to decrease with object size as  $1/R$  or with object mass as  $1/M^{1/3}$ .

The orbital migration rate due to gravitational interactions between an object and a disk increases with the mass of the object, as we will see in the next section. There is then a cross-over mass above which the orbital changes due to disk gravitational forces dominate over those due to drag forces. For typical parameters, this value is much less than an Earth mass,  $1M_{\oplus}$  (*Hourigan & Ward*, 1984). Consequently, for the purposes of planet migration, we will ignore the effects of aerodynamic gas drag.

### 2.2 Torques Due To Mildly Perturbed Particles

As an initial description of gravitational disk-planet interactions, we consider the disk to consist of noninteracting particles, each having mass  $M$  much less than the mass of the planet  $M_p$ . The disk is assumed to extend smoothly across the orbit of the planet without a gap. The planet is then in the Type I regime of planet migration, as discussed in the Introduction. The model leads to insights about several issues concerning planet migration. In particular, it explains why the migration rate increases with planet mass and allows us to estimate the magnitude of the migration rate. This estimated migration rate is numerically close to what more detailed calculations reveal for simple disk structures. The approximations fall short of allowing a determination of whether the migration is inward or outward and the determination of the detailed dependence of the migration rate on disk properties, such as the density and temperature distributions. The treatment describes material that orbits about the star and undergoes a small deflection by the planet. It does not describe the effects of material that lies very close to the planet in the so-called coorbital region, where the deflections are large (see Fig. 2). We will consider a model for that region in Section 2.3.

In this model, the particles are considered to encounter and pass by the vicinity of a planet that is on a fixed circular orbit of radius  $a$  about the star of mass  $M_s$ . As a result of their interactions, the planet and disk exchange energy and angular momentum. This situation is a special case of the famous three-body problem in celestial mechanics. The tidal or Hill radius of the planet where planetary gravitational forces dominate over stellar and centrifugal forces is

given by

$$R_H = a \left( \frac{M_p}{3M_s} \right)^{1/3}, \quad (2)$$

where radius  $R_H$  is measured from the center of the planet.

Consider a particle that approaches the planet on a circular orbit about the star with orbital radius  $r$  sufficiently different from  $a$  to allow it to freely pass by the planet with a small deflection. This condition requires that the closest approach between the particle and planet  $\sim |r - a|$  to be somewhat greater than a few times  $R_H$ . The solid line in Fig. 3 shows the path of a particle deflected by a planet whose mass is  $10^{-6}M_s$  (corresponding to 0.3 Earth masses for a planet that orbits a solar mass star), Hill radius  $R_H \simeq 0.007a$ , and orbital separation  $r - a \simeq 3.5R_H$ . The planet and particle orbit counter-clockwise in the inertial frame with angular speeds  $\Omega_p$  and  $\Omega(r)$ , respectively. In the frame of the planet, the particle moves downward in the figure, since its angular speed is slower than that of the planet ( $\Omega(r) < \Omega_p$  for  $r > a$ ).

To estimate the angular momentum change of a particle like that in Fig. 3, we consider a Cartesian coordinate system centered on the planet and corotates with it. The  $x$  axis lies along a line between the star and planet and points away from the star. We consider in detail the fate of a particle that starts its approach toward the planet on a circular orbit of orbital radius  $r$  that lies outside the orbit of the planet,  $x = r - a > 0$ . The planet and the pre-encounter particle are on circular Keplerian orbits whose orbital frequencies are given by equation (1). We later discuss what happens to particles that begin their encounter at orbital radii smaller than the planet's ( $x < 0$ ). The dashed line in Fig. 3 traces the path that the particle would take in the absence of the planet, while the solid line shows the path in the presence of the planet. In both cases, the particle paths are generally along the negative  $y$  direction. The two paths are nearly identical prior to the encounter with the planet (for  $y > 0$ ).

The particle velocity in the frame that corotates with the planet is then approximately given by

$$\mathbf{v} \simeq r(\Omega(r) - \Omega_p)\mathbf{e}_y \simeq xa \frac{d\Omega}{dr}\mathbf{e}_y \simeq -\frac{3}{2}\Omega_p x \mathbf{e}_y, \quad (3)$$

where  $x = r - a$ ,  $\Omega(r)$  is given by equation (1), and  $\Omega_p = \Omega(a)$ . Upon interaction with the planet, the particle is deflected slightly toward it. The particle of mass  $M$  experiences a force  $F_x = -GMM_p x / (x^2 + y(t)^2)^{3/2}$ . This force mainly acts over a time  $t$  when  $|y(t)| \lesssim x$  and is  $F_x \sim -GMM_p/x^2$ . From equation (3), it follows that the encounter time  $\Delta t \sim x/v \sim 1/\Omega_p$ , of order the orbital period of the planet, independent of  $x$ .

To proceed, we apply the so-called impulse approximation, as employed by *Lin & Papaloizou, 1979*. The approximation involves the assumption that the duration of the interaction is much shorter than the orbital period. Since the duration of the encounter is of order the orbital period, the approximation is only marginally satisfied. Consequently, the expressions we obtain cannot be determined with high

accuracy in this approximation. They contain the proper dependences on various physical quantities. But the approximation does not lead to the correct dimensionless numerical coefficients of proportionality for the angular momentum change of a particle. Therefore, we suppress the numerical coefficients in the analysis. An exact treatment in the limit of weak perturbations exerted by a small mass planet is given in *Goldreich & Tremaine, 1982*.

As a result of the encounter, the particle with  $x > 0$  acquires an  $x$  (radial) velocity

$$v_x \sim \frac{F_x \Delta t}{M} \sim -\frac{GM_p}{x^2 \Omega_p}. \quad (4)$$

The particle is then deflected by an angle

$$\delta \sim \frac{v_x}{v} \sim \left( \frac{M_p}{M_s} \right) \left( \frac{a}{x} \right)^3 \sim \left( \frac{R_H}{x} \right)^3 \quad (5)$$

after the encounter (see Fig. 3).

To determine the change in angular momentum of the particle, we need to determine its change in velocity along the  $\theta$  direction, that is the same as the  $y$  direction near the planet. To determine this velocity change,  $\Delta v_y$ , we ignore the effects of the star during the encounter, and apply conservation of kinetic energy between the start and end of the encounter in the frame of the planet. The velocity magnitude  $v$  is then the same before and after the encounter, although the direction changes by angle  $\delta$ . Since the particle in Fig. 3 moves in the negative  $y$  direction, its pre-encounter  $y$  velocity is  $-v$  and its post-encounter  $y$  velocity is  $-v \cos \delta$ . We then have that the change of the velocity of the particle along the  $y$  direction is

$$\Delta v_y = -v \cos \delta + v, \quad (6)$$

where  $v \simeq 1.5\Omega_p x$  is the magnitude of the velocity before the encounter (see equation (3)). We assume that the perturbation is weak,  $\delta \ll 1$ , and obtain from equations (3), (5), and (6)

$$\Delta v_y \sim v \delta^2 \sim a\Omega_p \left( \frac{M_p}{M_s} \right)^2 \left( \frac{a}{x} \right)^5. \quad (7)$$

It then follows that the change in angular momentum of the particle is given by

$$\Delta J \sim Ma\Delta v_y \sim Ma^2\Omega_p \left( \frac{M_p}{M_s} \right)^2 \left( \frac{a}{x} \right)^5. \quad (8)$$

Fig. 4 plots the orbital radius as a function of time for the particle plotted in Fig. 3, where  $t = 0$  is the time of closest approach to the planet. Notice that after the encounter, the particle orbit acquires an eccentricity, as seen by the radial oscillations, and an increased angular momentum, as seen by the mean shift of the radius for the oscillations. Although the particle is initially deflected inward (negative  $x$  direction, towards the star), as expected by equation (4), it rebounds after the encounter to an increased time-average

radius and higher angular momentum, as expected by equation (8).

Fig. 5 plots the torque on a particle due to the planet as a function of time, where  $t = 0$  is the time of closest approach between the particle and the planet. The solid curves are for particles that follow their actual paths (similar to the solid line in Fig. 3). The dashed curves are for particles that are made to follow the unperturbed paths (similar to the dashed line in Fig. 3). The net angular momentum change is the time-integrated torque. The torque on a particle along an unperturbed path (such as the dashed curve in Fig. 3) is antisymmetric in the time  $t$ . Consequently, there is no net change in angular momentum accumulated along this path. The change in angular momentum along the unperturbed path from  $t = -\infty$  to  $t = 0$  is linear in the planet mass, since the force due to the planet is proportional to its mass. The departures from antisymmetry of the torque versus time result in the net angular momentum change. These departures are a consequence of the path deflection (solid curve in Fig. 3).

For the case of the closer encounter plotted in the top panel of Fig. 6, the departures from the unperturbed case are substantial. But for a slightly larger orbit (bottom panel), the torque along the perturbed path differs only slightly from the torque along the unperturbed path that integrates to zero. This behavior is a consequence of the steep decline of  $\Delta J$  with  $x$  in equation (8). For  $x$  greater than a few  $R_H$ , the angular momentum change acquired before the encounter is nearly equal and opposite to the angular momentum change at later times  $t > 0$ . The net angular momentum change is given by equation (8) and is quadratic in the planet mass. The quadratic dependence on  $M_p$  is a consequence of the deviations in torque between the perturbed and the unperturbed paths, since the angular momentum change along the unperturbed path is zero. These deviations involve the product of the linear dependence of the force on planet mass with the linear dependence of the path deflection on planet mass (equation (5)) and so are quadratic in  $M_p$ . This quadratic dependence of torque on planet mass is important. It leads to the conclusion we obtain later that the migration rate of a planet is proportional to its mass.

The particle in Fig. 3 gains angular momentum, as predicted by equation (8). The reason is that the path deflection occurs mainly after the particle passes the planet, that is for  $y < 0$ . The deflection takes the particle closer to the planet than would be the case along the unperturbed path. The planet then pulls the particle toward positive  $y$ , causing it to gain angular momentum. Just the opposite would happen for a particle with  $r < a$ , for  $x < 0$  in equation (8). The particle would approach the planet in the positive  $y$  direction, be deflected towards the planet for  $y > 0$ , and be pulled by the planet in the negative  $y$  direction, causing it to lose angular momentum. The interaction behaves somewhat like friction. The particle gains (loses) angular momentum if it moves slower (faster) than the planet. The angular momentum then flows outward as a result of the interactions. That is, for a decreasing angular velocity with

radius ( $d\Omega/dr < 0$ ) as in the Keplerian case, a particle whose orbit lies interior to the planet gives angular momentum to the planet, since the planet has a lower angular speed than the particle. The planet in turn gives angular momentum to a particle whose orbit lies exterior to it.

The planet in effect pushes material away from its orbit. A particle outside the orbit of the planet is forced outward (in a time-averaged sense) as it gains angular momentum, and a particle inside is forced inward as it loses angular momentum. From this point of view, the gravitational effects of the planet behave in a repulsive manner.

Fig. 6 shows the results of numerical tests of equation (8). It verifies the dependence of  $\Delta J$  on  $x$  and  $M_p$ . Departures of the expected dependences (solid lines) occur when  $x \simeq 3R_H$ . At somewhat smaller values of  $x$ , the particle orbits do not pass smoothly by the planet. Instead, they lie within the coorbital region where they periodically undergo strong deflections, as seen in Fig. 2. We omit this region from current consideration and consider it later in Section 2.3.

We now determine the torque on the planet for a set of particles that form a continuous disk (of zero thickness) that lies in the orbit plane of the planet with surface density (mass per unit area)  $\Sigma$  that we take to be constant in the region near the planet. The particle disk provides a flux of mass (defined to be positive) past the planet between  $x$  and  $x + dx$

$$d\dot{M} \sim |v_y| \Sigma dx \sim \Sigma \Omega_p x dx. \quad (9)$$

We evaluate the torque  $T_{\text{out}}$  on the planet due to disk material that extends outside the orbit of the planet from  $r = a + \Delta r$  to  $\infty$  or  $x$  from  $\Delta r$  to  $\infty$ , where  $\Delta r > 0$ . We use the fact that the torque the planet exerts on the disk is equal and opposite to the torque the disk exerts on the planet. We then have

$$T_{\text{out}} \sim - \int_{\Delta r}^{\infty} \frac{\Delta J}{M} \frac{d\dot{M}}{dx} dx, \quad (10)$$

$$T_{\text{out}} = -C_T \Sigma a^4 \Omega_p^2 \left( \frac{M_p}{M_s} \right)^2 \left( \frac{a}{\Delta r} \right)^3, \quad (11)$$

where  $C_T$  is a dimensionless positive constant of order unity and  $\Delta J$  is evaluated through equation (8). The torque on the planet due to the disk interior to the orbit of the planet from  $x = -\infty$  to  $x = \Delta r$  with  $\Delta r < 0$  evaluates to  $T_{\text{in}} = -T_{\text{out}}$  or

$$T_{\text{in}} = C_T \Sigma \Omega_p^2 a^4 \left( \frac{M_p}{M_s} \right)^2 \left( \frac{a}{|\Delta r|} \right)^3. \quad (12)$$

The equations of motion for particles subject to only gravitational forces are time-reversible. We saw that particle in Fig. 3 gains angular momentum from its interaction with the planet. But, if we time-reverse the particle-planet encounter in Fig. 3, we see that the eccentric orbit particle would approach the planet (both on clockwise orbits) and then lose angular momentum (apply  $t \rightarrow -t$  in Fig. 4). What determines whether a disk particle gains or

loses angular momentum? We have assumed that the particles always approach the perturber on circular orbits. The particles periodically encounter the gravitational effects of the planet. The closer the particle orbits to the planet, the smaller the relative orbital speeds and the longer the time between encounters. From equation (3), it follows that the time between encounters  $\tau \simeq 2\pi a/v$  is estimated as

$$\tau \sim \frac{aP}{|x|}, \quad (13)$$

where  $P$  is the planet orbital period. Since the encounters are close  $|x| \ll a$ , the time between encounters is long compared to the encounter time  $\sim P$ , that is  $\tau \gg P$ . But we saw in Fig. 4 that the particles acquire eccentricity after the encounter. For this model to be physically consistent, we require that this eccentricity damp between encounters with the planet. The eccentricity damping produces an arrow of time for the angular momentum exchange process that favors circular orbits ahead of the encounter as shown in Fig. 3, resulting in a gain of angular momentum for particles that lie outside the orbit of the planet.

Equations (11) and (12) have important consequences. The torques on the planet arising from the inner and outer disks are quite powerful and oppose each other. This does not mean that the net torque on the planet is zero because we have assumed perfect symmetry across  $r = a$ . The symmetry is broken by higher order considerations. For this reason, migration torques are often referred to as differential torques.

Since the torques are singular in  $\Delta r$ , they are dominated by material that comes close to the planet. Consequently, the asymmetries occur through differences in physical quantities at radial distances  $\Delta r$  from the planet. In a gaseous disk, the effects of both temperature and density variations in radius can play a role in the asymmetry, as well as asymmetries associated with the differential rotation of the disk. We cannot describe the asymmetries due to temperature in this model because temperature is not described by the ballistic particles. For this simple model of a (pressure-free) particle disk, we consider for example the effect of the density variation in radius that we have ignored up to this point, although the other asymmetries are important. It does not matter which quantity is considered for the purposes of obtaining a rough expression for the net torque.

We expand the disk density in a Taylor expansion about the orbit of the planet and obtain that

$$\Sigma_{\text{out}} - \Sigma_{\text{in}} \simeq 2\Delta r \frac{d\Sigma}{dr}, \quad (14)$$

where  $\Sigma_{\text{in}}$  and  $\Sigma_{\text{out}}$  are the surface densities at  $r = a - \Delta r$  and  $r = a + \Delta r$ , respectively. Consequently, for  $|d\Sigma/dr| \sim \Sigma_p/a$ , we expect that the sum of the inner and outer torques to be smaller than their individual values by an amount of order  $\Delta r/a$ . Similar considerations apply to variations in other quantities. That is, we have that the absolute value of the net torque  $T$  on the planet is approximately given by

$$|T| = |T_{\text{in}} + T_{\text{out}}|, \quad (15)$$

$$\sim |T_{\text{in}}| \frac{|\Delta r|}{a}, \quad (16)$$

$$\sim \Sigma \Omega_p^2 a^4 \left( \frac{M_p}{M_s} \right)^2 \left( \frac{a}{|\Delta r|} \right)^2. \quad (17)$$

The above equation for the torque (equation (17)) must break down for small  $\Delta r$ , in order to yield a finite result. For values of  $|\Delta r| \lesssim 3R_H$ , the particles become trapped in closed orbits in the so-called coorbital region (see Fig. 2). We exclude this region from current considerations, since the torque derivation we considered here does not apply in this region. In particular, the assumption that particles pass by the planet with a small deflection is invalid in this region. Using equation (17) with  $|\Delta r| \sim R_H$ , we obtain a torque

$$|T| \sim \Sigma \Omega_p^2 a^4 \left( \frac{M_p}{M_s} \right)^{4/3}. \quad (18)$$

Another limit on  $\Delta r$  comes about due to gas pressure. One effect of gas pressure is to cause the disk to have a nonzero thickness  $H$ . The disk thickness is measured by its scale height out of the orbital plane. The disk scale height is determined by the force balance in the direction perpendicular to the orbit plane, the  $z$  or vertical direction. Gas pressure forces act to spread the gas in this direction, while gravitational forces act to confine it. We consider the vertical structure of an axisymmetric disk, unperturbed by a planet. There are no motions in the vertical direction and the disk is said to be in hydrostatic balance.

The vertical hydrostatic balance condition can be written as

$$\frac{\partial p(r, z)}{\partial z} = \rho g_z, \quad (19)$$

where  $p(r, z)$  is the gas pressure,  $\rho(r, z)$  is the gas density, and  $g_z(r, z)$  is the vertical gravity. The vertical gravity is the  $z$  component of the gravitational force per unit disk mass due to the star that is equal to

$$g_z(r, z) = -\frac{GM_s z}{r^3} = -\Omega^2(r) z, \quad (20)$$

where  $\Omega$  is given by equation (1). For a vertically isothermal disk, a disk whose temperature and therefore sound speed  $c(r)$  is independent of  $z$ , we have

$$p(r, z) = \rho(r, z) c^2(r). \quad (21)$$

Substituting equations (20) and (21) into equation (19), we obtain

$$\rho(r, z) = \rho(r, 0) \exp\left(-\frac{z^2}{2H^2}\right) \quad (22)$$

and

$$H(r) = \frac{c(r)}{\Omega(r)}, \quad (23)$$

where  $c$  is the gas sound speed that is a function of disk temperature. Disk thickness  $H$  is a measure of the importance of gas pressure. For conditions in protostellar disks,

the disk thickness to radius ratio (disk aspect ratio) is typically  $0.03 \lesssim H/r \lesssim 0.1$ , corresponding to a gas sound speed of about  $1.5 \text{ km s}^{-1}$  at 1AU from a solar mass star.

For an axisymmetric disk of nonzero thickness, the surface density  $\Sigma = \int_{-\infty}^{\infty} \rho dz$  evaluates to

$$\Sigma(r) = \int_{-\infty}^{\infty} \rho(r, z) dz = \sqrt{2\pi} H(r) \rho(r, 0), \quad (24)$$

where  $\rho(r, z)$  is defined by equation (22). The gas density is in effect smeared over distance  $H$  out of the orbit plane. Near the planet, the gas gravitational effects are then smoothed over distance  $H$ . Distance  $\Delta r$  is in effect limited to be no smaller than  $\sim H$ . For  $\Delta r \sim H$ , the torque expression (17) is then estimated as

$$|T| \sim \Sigma \Omega_p^2 a^4 \left( \frac{M_p}{M_s} \right)^2 \left( \frac{a}{H} \right)^2. \quad (25)$$

Which form of the torque applies (equation (18) or (25)) to a particular system depends on the importance of gas pressure. For  $H < R_H$ , gas pressure effects are small compared to the gravitational effects of the planet near the Hill radius. Consequently, we expect equation (18) to be applicable in the case of relatively weak gas pressure,  $H < R_H$ , and equation (25) to be applicable otherwise. For typically expected conditions in gaseous protostellar disks, it turns out that equation (25) is the relevant one for planets undergoing Type I migration.

The migration rate  $\dot{r}_p/a = T/J_p$  for a planet with angular momentum  $J_p$  is then linear in planet mass, since  $T$  is quadratic while  $J_p$  is linear in planet mass. Therefore, the Type I migration rate increases with planet mass, as asserted in Section 2.1. This somewhat surprising result that more massive planets migrate faster is in turn a consequence of the quadratic variation of  $\Delta J$  with planet mass in equation (8). This quadratic dependence occurs because the possible linear dependence of  $\Delta J$  on planet mass vanishes due to the antisymmetry of the torque as a function of time along the unperturbed particle path, as discussed after equation (8).

Based on equation (25) with typical parameters for the minimum mass solar nebula at the location of Jupiter  $a = 5\text{AU}$  ( $\Sigma = 150 \text{ g cm}^{-2}$ ,  $\Omega = 1.8 \times 10^{-8} \text{ s}^{-1}$ , and  $H = 0.05a$ ), we estimate the planetary migration timescale  $J_p/T$  for a planetary core of 10 Earth masses embedded in a minimum mass solar nebula as  $4 \times 10^5 \text{ yr}$ . This timescale is short compared to the disk lifetime, estimated as several times  $10^6 \text{ yr}$ , or the Jupiter formation timescale of  $\gtrsim 10^6 \text{ yr}$  in the core accretion model. The relative shortness of the migration timescale is a major issue for understanding planet formation. Since migration is found to be inward for simple disk models, as we will see later, the timescale disparity suggests that a planetary core will fall into the central star before it develops into a gas giant planet. Research on planet migration has concentrated on including additional effects such as gas pressure and on improving the migration rates by means of both analytic theory and multi-dimensional simulations.

A more detailed analysis reveals that the torque in equation (25) does provide a reasonable estimate for the magnitude of migration rates in gaseous disks in the so-called Type I regime in which a planet does not open a gap in the disk. However, the derivation of the torque in this section is not precise enough to determine whether the migration is inward or outward (i.e., whether  $T$  is negative or positive). The density asymmetry about  $r = a$  (see equation (14)) typically involves a higher density at smaller  $r$ , as in the case of the minimum mass solar nebula. This variation suggests that torques from the inner disk dominate, implying outward migration, as was thought to be the case in early studies. But this conclusion is incorrect. As we will discuss later, inward migration is typically favored, at least for simple disk models. We have not included the effects of gas temperature and gas pressure. A disk with gas pressure propagates density waves launched by the planet. The analysis in this section has only considered effects of material that passes by the planet. In addition, there are effects from material that lies closer to the orbit of the planet (see Fig. 2). This region can also provide torques. We have also assumed that the disk density is undisturbed by presence of the planet. Feedback effects of the disk disturbances and gaps in the disk can have an important influence on migration. Finally, there are other physical effects such as disk turbulence that should be considered. We will consider such effects in subsequent sections.

### 2.3 Coorbital Torques

Thus far we have considered torques that arise from gas that passes by the planet in the azimuthal direction (the  $y$  direction in Fig. 3) with a modest deflection. Gas that resides closer to the planet,  $|r - a| \lesssim 3R_H$ , in the so-called coorbital region, does not pass by the planet. Instead, it follows what are called librating orbits in the corotating frame of the planet as seen in Fig. 2. We will consider librating orbits of particles that reach close to a planet that lies on a fixed circular orbit, the so-called horseshoe orbits. A particle at position  $o+$  in Fig. 2 is in circular motion outside the orbit of the planet. It moves more slowly than the planet and approaches it. The particle in this case is more strongly perturbed by the planet than the more distant particle in Fig. 3. It gets pulled inward by the planet, causing it to change to a circular orbit interior to the planet's orbit once it reaches position  $i+$ . Since the particle is now moving faster than the planet, it moves away from it. In the process, the particle has executed a U-turn. At a later time, the particle approaches the planet from behind, at position  $i-$ , and the planet pulls the particle outward, causing it to make a second U-turn to position  $o-$ . The particle is then back to the initial outer radius that it started on before both encounters. The particle path is closed in the corotating frame of the planet.

With each change in angular momentum of the particle, there is an equal and opposite change in angular momentum of the planet. But, whatever angular momentum is gained

by a particle as it changes from the inner radius  $r_i$  to outer radius  $r_o$  is lost when it later encounters the planet and shifts from  $r_o$  to  $r_i$ . The reason is that the particle follows a periodic orbit in the frame of the planet, so there is no change in angular momentum over a complete period of its motion. As a result, angular momentum changes do not grow over long timescales. At any instant, the largest angular momentum change possible over any time interval is that acquired in the last particle-planet encounter. Therefore, the time-averaged torque on the planet due to a particle drops to zero over timescales longer than the period of its motion. So although particles on closed horseshoe orbits can come close to the planet, the orbital symmetry limits the torque that they exert on the planet.

For a set of particles, there is a further type of torque cancellation that occurs. Recall that the time period between particle-planet encounters (the libration timescale) varies inversely with the particle-planet orbital separation as  $1/x$  (see equation (13)). So even if a set of particles at different radii are initially lined up to encounter the planet at the same time and produce a large torque, they will eventually drift apart in azimuth (phase) and encounter the planet at different times. After a while, at a time when one particle gains angular momentum another will be losing it. This randomization, called "phase mixing", leads to a drop in torque over time. Fig. 7 shows the angular momentum evolution of a set of 60 particles that initially lie on the negative  $x$  axis within the horseshoe orbit region exterior to the orbit of the planet ( $r > a$ ). The torque (the derivative of the curve) shows both types of cancellations: the time rate of change of angular momentum oscillates due to the orbital symmetry and the amplitude of the oscillations decreases due to phase mixing.

A space-filling continuous set of small particles will be considered to represent coorbital gas. The disk in this case is dissipationless and pressureless, and the planet is on a fixed circular orbit. As is the case for a set of particles described above, the torque that the gas exerts on the planet approaches zero on timescales longer than the time for gas to make successive encounters with the planet.

We now consider the torque caused by gas whose density varies with radius with some imposed initial surface density distribution  $\Sigma(r)$ . The particle paths in Fig. 2 then become streamlines for the gas flow. Gas loses angular momentum in going from position  $o+$  to  $i+$ . This angular momentum is continuously gained by the planet. Similarly, the planet continuously loses angular momentum from the gas that passes from  $i-$  to  $o-$ . The gas spends a relatively short time in transition between  $r_i$  and  $r_o$  compared to the time it spends between encounters given by equation (13), where  $x = a - r_i$ . We consider here the torque exerted on the planet on timescales longer than the transition timescale, but shorter than the timescale between encounters with the planet.

As gas in the coorbital region approaches from inside the orbit of the planet, it carries a mass flux (defined to be

positive) that we estimate as

$$\dot{M}_i \sim \Sigma_i |\Omega_i - \Omega_p| r_i w_i, \quad (26)$$

where  $w_i$  denotes the radial extent (width) of the coorbital horseshoe region interior to the planet's orbital radius. Quantities  $\Sigma_i$ ,  $\Omega_i$ , and  $r_i$  denote the values of the surface density, angular velocity, and orbital radius, respectively, at position  $i-$ . This position lies at an intermediate radius within the horseshoe orbit region and interior to the planet's orbit. Gas at this position is executing circular motion, just ahead of an encounter with the planet. Similarly, for coorbital gas outside the orbit of the planet, the mass flux is estimated by

$$\dot{M}_o \sim \Sigma_o |\Omega_o - \Omega_p| r_o w_o, \quad (27)$$

where the subscripts denote the values at a point  $o+$  that lies at an intermediate radius within the horseshoe orbit region outside the orbit of the planet.

Due to the orbital geometry, we have that region widths satisfy  $w_i \sim w_o \sim r_o - a \sim a - r_i$ . This gas interacts with the planet and undergoes a change in angular momentum per unit mass as it flows from position  $i-$  to  $o-$

$$\Delta J = r_o^2 \Omega_o^2 - r_i^2 \Omega_i^2 \sim a \Omega_p^2 w > 0, \quad (28)$$

where  $w = w_o + w_i \sim r_o - r_i$ . In going from  $o+$  to  $i+$ , the gas undergoes an equal and opposite change in angular momentum,  $-\Delta J$ . The flows from outside and inside the orbit of the planet impart a torque on the planet. This torque is equal and opposite to the rate of change of angular momentum of gas resulting from the two contributing mass fluxes

$$T_{co} = (\dot{M}_o - \dot{M}_i) \Delta J \quad (29)$$

$$\sim \dot{M}_o \left( 1 - \frac{\dot{M}_i}{\dot{M}_o} \right) a \Omega_p^2 w. \quad (30)$$

We need to be careful in evaluating the ratio of the mass fluxes in the above equation, since departures from unity are critical. From equations (26) and (27), the ratio of the mass fluxes is given by

$$\frac{\dot{M}_i}{\dot{M}_o} = \frac{\Sigma_i}{\Sigma_o} \left( \frac{|\Omega_i - \Omega_p| r_i w_i}{|\Omega_o - \Omega_p| r_o w_o} \right). \quad (31)$$

*Ward, 1991* showed that the term in parenthesis on the right-hand side is equal to  $B_o/B_i$ , where  $B(r)$  is the Oort constant defined through  $2rB = d(r^2\Omega)/dr$  and  $B(r) = \Omega(r)/4$  for a Keplerian disk. We then obtain that

$$\frac{\dot{M}_i}{\dot{M}_o} = \frac{\Sigma_i B_o}{\Sigma_o B_i}. \quad (32)$$

Using equation (27), we then approximate  $\dot{M}_o$  appearing in the first term on the right-hand side of equation (30) as

$$\dot{M}_o \sim \Sigma \Omega_p a w^2. \quad (33)$$



Applying equations (30), (32), and (33), we then obtain an expression for the coorbital torque as

$$T_{\text{co}} \sim \Sigma \Omega_{\text{p}}^2 a w^3 \left( \frac{\Delta \Sigma}{\Sigma} - \frac{\Delta B}{B} \right), \quad (34)$$

$$\sim \Sigma \Omega_{\text{p}}^2 w^4 \frac{d \log(\Sigma/B)}{d \log r}, \quad (35)$$

where  $\Delta \Sigma = \Sigma_{\text{o}} - \Sigma_{\text{i}}$  and  $\Delta B = B_{\text{o}} - B_{\text{i}}$ .

Quantity  $B/\Sigma$  is sometimes called the vortensity, since  $B$  is half the vorticity, that is half the curl of the unperturbed velocity  $r\Omega e_{\theta}$ . The coorbital torque then depends on the gradient of the vortensity. Recall that in this situation, the torque is not permanent. It oscillates and decays to zero, due to phase mixing, as discussed above. The coorbital torque drops to zero or is said to be saturated on long timescales. The gas density in the coorbital region becomes modified over time so that the vortensity becomes constant and the torque approaches zero.

Gas that flows on the closed streamlines shown in Fig. 2 can impart a change in angular momentum on the planet that is at most about equal to the gas angular momentum of the region times its fractional width,  $w/a$  (that is,  $\Sigma \Omega_{\text{p}} a^2 w^2$ ). This angular momentum change is due to the rearrangement of gas within the horseshoe orbit region from some initial state. In this model, gas is trapped within the coorbital region and cannot exchange angular momentum with the large reservoir in the remainder of the disk. Maintaining a coorbital torque over long timescales requires the action of a process that breaks the symmetry of the streamlines and permits exchange with the remainder of the disk. One such process involves the disk turbulent viscosity. The disk viscosity acts to establish a characteristic density distribution, as discussed in the Introduction. Sufficiently strong turbulence can overcome the effects of phase mixing that saturate the torque. The torque is then given by equation (35), where the density distribution  $\Sigma(r)$  is determined by turbulent viscosity in the viscous accretion disk. The vortensity gradient is then maintained at a nonzero value. The angular momentum changes within the coorbital region are transferred to the remainder of the disk through torques associated with frictional stresses caused by disk turbulent viscosity (viscous torques). In this way, a steady state torque can be exerted on the planet over timescales much longer than the libration timescale  $\sim aP/w$ .

We compare the coorbital torque with the net torque due to particles outside the coorbital region in a pressureless disk, as we discussed in Section 2.2. Taking  $w \sim R_{\text{H}}$  in equation (35), we see that the unsaturated coorbital torque (taking  $|d \log(B/\Sigma)/d \log r| \sim 1$  and nonzero) is comparable to the torque due to particles outside the coorbital region in equation (18). It can be shown that this is also true for a disk where pressure effects are important, where  $H > R_{\text{H}}$ . For such a disk, the coorbital torque is generally of the same order as the net torque from the region outside the coorbital zone, equation (25). The direction of the coorbital torque contribution depends on the sign of the vortensity gradient. For the minimum mass solar nebula model,

$\Sigma \propto r^{-3/2}$  and  $B \propto r^{-3/2}$ . Consequently, the coorbital torque is zero in that case. With more general density distributions of the form

$$\Sigma \propto r^{-\beta} \quad (36)$$

and for smaller values of  $\beta < 3/2$ , the coorbital torque on the planet is positive.

We have discussed how the disk turbulent viscosity can cause a torque to be exerted in the coorbital region over long timescales. But if the amount of viscosity is too small, the phase mixing process discussed above can dominate and cause the torque to saturate. For the turbulent viscosity to prevent torque saturation, the timescale for turbulence to affect the density in the coorbital region needs to be shorter than the libration timescale on which the torque would drop in a nonviscous disk. This criterion imposes a constraint on the level of viscosity required. So although they are potentially powerful, coorbital torques are not guaranteed to play a role in planet migration in all cases.

Although the coorbital torque is of the same order as the net torque due to material outside the orbital zone, more detailed calculations as described in the next section show it typically does not dominate the total torque, at least for simple disk conditions.

Although the description here is self-consistent, coorbital torques are less well understood than the torques involving noncoorbital material we considered in Section 2.2. They are more complicated because they are subject to saturation. The asymmetry in the coorbital region that prevents torque saturation can in principle be produced by effects other than turbulence, such as the migration of the planet itself (see Section 3.2). Furthermore, recent simulations suggest that the thermodynamic state of the gas, not considered in this model, can modify the coorbital torque and possibly result in outward migration, as is discussed in Section 3.2.

## 2.4 Type I Migration

The torques arising from gas that lies somewhat inside the orbit of the planet  $r < a$  (but outside the coorbital region) act to cause outward migration, while torques arising from gas outside the orbit of the planet act to cause inward migration, as discussed in Section 2.2. The net migration torque was estimated in equation (25). But due to the inaccuracy of the approximations, the sign of the torque and its dependence on gas properties, such as the density and temperature distributions, could not be determined. More accurate analytic calculations of the torque involve solving the fluid equations for gas subject to the gravitational perturbing effects of the planet. Both the weakly perturbed region (Section 2.2) and coorbital region (Section 2.3) are analyzed. The calculations described in this section assume a simple disk model. By a simple model we mean that the disk has smooth disk density distribution, in the absence of the planet, and a smooth and fixed temperature distribution, even in the presence of the planet.

Consider a cylindrical coordinate system centered on the star  $(r, \theta, z)$ . In these calculations, the perturbing potential of a circular orbit planet is expanded in a Fourier series as

$$\Phi(r, \theta, t) = \sum_m \Phi_m(r, a) \cos[m(\theta - \Omega_p t)], \quad (37)$$

where  $m$  is a nonnegative integer, and  $\Omega_p$  is the orbital frequency of the planet. Such an expansion is possible because the potential is periodic in azimuth and periodic in time with the planet's orbital period. In addition, at fixed radius  $r$  (and fixed  $a$ ), the potential depends only on the relative azimuth between that of a point  $\theta$  and that of the planet  $\Omega_p t$ , that is  $\theta - \Omega_p t$ . For each azimuthal wavenumber  $m$ , the gas response is calculated by means of linear theory. There is a torque associated with each  $m$ -value due to the effects of the density perturbation for each  $m$ . The sum of these torques determine the net torque on the planet.

The results show that the gas response is dominated by the effects of resonances (*Goldreich & Tremaine, 1979, 1980*). There are two types of resonances that emerge: Lindblad resonances and corotational resonances. They occur in the regions described in Sections 2.2 and 2.3, respectively. Such resonances also arise in the theory of the spiral structure of galaxies and planetary rings.

The gas response to a particular Fourier potential component  $m$  in equation (37) is strong at particular radii  $r_m$  where the Lindblad resonance condition is satisfied. The Lindblad resonances occur for gas that periodically passes by the planet. They correspond to the so-called mean motion resonances of particles in celestial mechanics. For a given  $m$ -value, the forcing frequency experienced by a particle is the time derivative of the argument of the  $\cos$  function in equation (37) along a particle's path  $\theta(t)$ . The forcing frequency is then given by  $m(\Omega(r) - \Omega_p)$ . Consider a particle in a circular orbit about a central mass. If the particle is momentarily slightly perturbed, it oscillates radially at a frequency called the epicyclic frequency, often denoted by  $\kappa(r)$ . This frequency is the free oscillation frequency of the particle, analogous to the free oscillation frequency of a spring in a simple harmonic oscillator. For a Keplerian disk, the radial frequency  $\kappa(r)$  is equal to the circular frequency  $\Omega(r)$ . (This is why noncircular Keplerian orbits are closed ellipses in the inertial frame.) Lindblad resonances occur wherever the absolute value of the forcing frequency matches the free oscillation frequency. For a Keplerian disk, the Lindblad resonance condition,  $|m(\Omega - \Omega_p)| = \kappa$ , simplifies to

$$\Omega(r_m) = \frac{m\Omega_p}{m \mp 1}, \quad (38)$$

where  $\Omega(r)$  is given by equation (1).

For each  $m$ -value there are two Lindblad resonances. An outer Lindblad resonance (OLR) occurs outside the orbital radius of the planet, for which the plus sign is taken in the denominator of equation (38) and an inner Lindblad resonance (ILR), for which the minus sign is taken (see Fig. 8). At each Lindblad resonance, spiral waves are launched that

propagate away from the resonance (see Fig. 9). These waves are similar to acoustic waves, but are modified by the disk rotation. One can associate an angular momentum and energy with the waves. They carry energy and angular momentum from the planet, resulting in a torque on the planet. Various processes cause these waves to damp as they propagate. As the waves damp, their angular momentum is transferred to the disk. This situation is reminiscent of the case of ocean waves. They are generated by wind far from land, but undergo final decay when they break at the shore and can cause irreversible changes. Similarly, the waves in disks can modify the underlying disk density distribution  $\Sigma(r)$  and open gaps as they damp, although the disk turbulence can wash out these effects.

At the corotation resonance in a Keplerian disk, the condition is simply that

$$\Omega(r_m) = \Omega_p, \quad (39)$$

or  $r_m = a$  for all  $m$ . That is, the corotation resonance occurs at the orbital radius of the planet. It lies in the region of orbits shown in Fig. 2. The corotation resonance also creates disturbances in the disk, but the disturbances do not propagate. Instead they are evanescent and remain trapped within a radial region whose size is of order the disk thickness  $H$ .

The analytic calculations determine a torque for each  $m$ -value at the inner and outer Lindblad resonances and the corotation resonance. The strength of the Lindblad torques increases for resonances that lie closer to the planet. The closer resonances occur for higher  $m$ -values. But due to effects of pressure, the resonance condition (38) breaks down close to the planet and the torque reaches a maximum value for  $m_{cr} \sim r/H$  where the resonance is at a distance of order the disk thickness from the planet (see Fig. 8). Three dimensional effects also weaken the torque close to the planet. The reduction arises because the gas is spread over the disk thickness  $H$  (as was discussed in Section 3.2). The critical  $m$ -value of  $m_{cr}$  is sometimes called the torque cutoff. This reduction of torque for  $m > m_{cr}$  implies that the sum of the torques over all  $m$ -values remains finite. In this way, these calculations avoid the singularity that we encountered in equation (17) involving  $\Delta r$ .

The results of these calculations show that planets have a definite tendency to migrate inward (*Ward, 1997*). For a given  $m$ -value, the torque is stronger at the OLR than the ILR in a disk, even if we ignore the asymmetries caused by density and temperature variations. There are several contributions to this density- and temperature-independent effect. One such contribution can be seen by noticing that for a given  $m$ , the OLRs lie slightly closer to the planet's orbital radius than ILRs in equation (38). This asymmetry, as well as other density- and temperature-independent effects, enhances the inward migration effects caused by OLRs over the outward migration effects that are caused by ILRs. With simple disk structures (smooth disk density distributions and smooth, fixed temperature distributions),

such effects often dominate the overall torque on the planet for typical density and temperature distributions.

Density and temperature effects can also play an important role in determining the Lindblad torque. The surface density distribution in radius influences the torque balance in at least two ways. It affects the amount of gas at each resonance and it affects the radial pressure force. These two effects typically act in opposition to each other and partially cancel. A declining surface density distribution with radius, as is typical, places more gas at the ILRs than the OLRs. This effect provides an outward torque contribution, since the ILR torques are enhanced. Pressure effects typically cause the gas at orbital radius close to  $a$  to rotate a little more slowly than the planet, as discussed in Section 2.1. Although the primary effect here is gravitational and not gas drag as in Section 2.1, the gravitational torque on the planet again produces a qualitatively similar effect as drag and acts to cause inward migration. This effect can also be understood in terms of a slightly decreased angular velocity  $\Omega(r)$  (below the Keplerian rate) in equation (38) that causes both the ILRs and OLRs to move inward. The ILRs are then shifted away from the planet, while the OLRs are shifted towards it. The effect of pressure is to favor the OLRs, which contribute to inward migration.

The temperature distribution in radius also has multiple effects on the Lindblad torque balance. It affects the gas radial pressure force in a similar way that the density distribution does, as just described. The pressure effects of a radially declining temperature then contribute to inward migration. Temperature variations also modify the torque cutoff  $m_{\text{cr}} \sim a/H$ , since disk thickness  $H$  depends on the gas sound speed and therefore temperature (see equation (23)). The OLRs, being at a lower temperature (smaller  $H$ ) than the ILRs, have a higher cutoff  $m_{\text{cr}}$ . This effect favors the OLRs and its inward torques. Both effects of a declining temperature with radius, also generally expected, contribute to inward migration.

Detailed 3D linear analytic calculations of the Type I migration rates have been carried out by *Tanaka et al*, 2002. They assumed that the gas sound speed is strictly constant in radius. That is, the gas temperature is assumed to be unaffected by the planetary perturbations. For the case of saturated (zero) coorbital corotation torques, where only differential Lindblad torques are involved, the torque on the planet is given by

$$T = - (2.34 - 0.10 \beta) \Sigma(a) \Omega(a)^2 a^4 \left( \frac{M_{\text{p}}}{M_{\text{s}}} \right)^2 \left( \frac{a}{H} \right)^2, \quad (40)$$

where  $\beta$  is given by equation (36).<sup>1</sup> The torque on the planet resulting from the action of both Lindblad and (unsaturated)

<sup>1</sup>A higher sensitivity to density gradients (more negative coefficient of  $\beta$ ) was found in the analysis by *Menou & Goodman*, 2004.

coorbital corotation resonances is given by

$$T = - (1.36 + 0.54 \beta) \Sigma(a) \Omega(a)^2 a^4 \left( \frac{M_{\text{p}}}{M_{\text{s}}} \right)^2 \left( \frac{a}{H} \right)^2. \quad (41)$$

These migration rates are consistent with the estimate in equation (25). Numerical values for migration timescales based on equation (41) are plotted in Fig. 1. As mentioned above, temperature variations can also contribute to planet migration, but are not included in this treatment. Other results (such as the 2D calculation by *Ward*, 1997) suggest that the temperature variation should provide an additional term within the first parenthesis on the right-hand sides of equations (40) and (41) that is  $\sim \chi$ , where

$$T(r) \propto r^{-\chi} \quad (42)$$

is the temperature distribution with radius (not to be confused with torque). We typically expect in a disk that  $0 < \beta < 1.5$  and that  $0.5 \lesssim \chi < 0.75$ . Consequently, the migration is predicted to be inward and of order the rate that would be obtained even if density and temperature gradients ( $\beta$  and  $\chi$ ) were ignored. But, such gradients may take on different values than assumed here and potentially play an important role in slowing migration, as will be discussed in Section 3.1. In addition, some further effects, such as gas entropy gradients, can modify the coorbital torque. Recent studies have suggested that such thermal effects could change Type I migration and may even lead to outward migration (Section 3.1; *Paardekooper & Mellema*, 2006).

In comparing the saturated coorbital torque (equation (40)) to the unsaturated coorbital torque (equation (41)), we see that the effects of the coorbital torque reduce the inward migration rate for  $\beta < 1.5$  and nearly vanish for  $\beta = 1.5$ . This behavior is consistent with equation (35), using the fact that  $B \propto r^{-1.5}$ . The coorbital torque is then positive for  $\beta < 1.5$  and is zero for  $\beta = 1.5$ .

Nonlinear 3D hydrodynamical calculations have been carried out to test the migration rates, under similar disk conditions (in particular, local isothermality) used to derive the analytic model. Figs. 1 and 10 show that the migration rates agree well with the expectations of the theory.

We examine the comparison between simulations and theory in more detail by comparing torque distributions in the disk as a function of disk radius. We define the distribution of torque on the planet per unit disk mass as a function of radius as  $dT/dM(r) = 1/(2\pi r \Sigma(r)) dT/dr(r)$ . Fig. 11 plots  $dT/dM$  (scaled as indicated in the figure) as a function of radial distance from the planet based on 3D simulations. The distributions show that the region interior (exterior) to the planet provides a positive (negative) torque on the planet, as predicted in equations (11) and (12) for a particle disk. Also, the integrated total torque is negative, implying inward migration. The theory predicts that the torque density peak and trough occur at distance from the planet  $r - a = \Delta r \sim \mp H$ , where the torque cutoff takes effect. For the case plotted in Fig. 11 that adopts

$H = 0.05r$ , the predicted locations agree well with the locations of the peaks and troughs in the figure. Furthermore, the torque and torque density should scale with the square of the planet mass. Although the vortensity gradient is not small, since  $\Sigma/B \sim r$ , we do not find large contributions to the torque density from the coorbital region, as is also expected. As seen in Fig. 11, this expectation is well met for the two cases plotted.

## 2.5 Type II migration

The planet's tidal torques cause material interior to the orbit of the planet (not in the coorbital region) to lose angular momentum and material exterior to the orbit of the planet to gain angular momentum, as we saw in Section 2.2. The torques then act to clear a gap about the orbit of the planet. As discussed in the Introduction, Type II migration occurs when the planet mass is sufficiently large that tidal forces cause a gap to clear about the orbit of the planet (Lin & Papaloizou, 1986). The tidal torques on the disk interior or exterior to the planet are estimated by equation (11) with  $\Delta r \sim H$ . The tidal torque on the disk that acts to open the gap is then estimated as

$$T_o \sim \Sigma \Omega_p^2 a^4 \left( \frac{M_p}{M_s} \right)^2 \left( \frac{a}{H} \right)^3. \quad (43)$$

Turbulent viscosity acts to close the gap. The effects of turbulence are often described in terms of a kinematic viscosity  $\nu$  that is parameterized in the so-called  $\alpha$ -disk model as

$$\nu = \alpha cH, \quad (44)$$

where  $\alpha$  is a dimensionless number,  $c$  is the gas sound speed, and  $H$  is the disk thickness, described by equation (23) (Shakura & Sunyaev, 1973). The value of the key quantity  $\alpha$  is expected to be less than unity because we presume that the turbulent motions are slower than sonic and that the characteristic length scales for the turbulence are smaller than the disk thickness.

The turbulent viscosity provides a torque to close the gap

$$T_c \sim \frac{M_g \Delta J_g}{t_g}, \quad (45)$$

where  $M_g$  is the mass supplied by the disk in closing the gap,  $\Delta J_g$  is the change in the disk angular momentum per unit mass required to close the gap, and  $t_g$  is the time for gap closing. We estimate these quantities as

$$M_g \sim \Sigma a w, \quad (46)$$

$$\Delta J_g \sim a \Omega_p w, \quad (47)$$

$$t_g \sim \frac{w^2}{\nu}, \quad (48)$$

where  $w$  is the radial extent of the gap,  $\Sigma$  is the disk density just outside the gap, and  $\nu$  is the disk kinematic turbulent viscosity. The gap closing timescale estimate  $t_g$  is

based on the idea that the viscosity acts on a radial diffusion timescale across a distance  $w$ , which then implies the quadratic dependence on  $w$ . Applying this last set of relations to equation (45), we obtain that

$$T_c \sim \Sigma a^2 \Omega_p \nu, \quad (49)$$

independent of  $w$ .

In order to open a gap in the disk, the gap opening torque must be greater than the gap closing torque,  $T_o \gtrsim T_c$ . We then obtain a condition on the planet mass required to open a gap

$$\frac{M_p}{M_s} \gtrsim C_g \left( \frac{\nu}{a^2 \Omega_p} \right)^{1/2} \left( \frac{H}{a} \right)^{3/2}, \quad (50)$$

where  $C_g$  is a dimensionless number of order unity. Lin & Papaloizou, 1986 estimated that  $C_g = 2\sqrt{10}$ . For disk parameters  $\alpha = 0.004$  and  $H/r = 0.05$ , the predicted gap opening at the orbit of Jupiter about a solar mass star occurs for planets having a mass  $M_p \gtrsim 0.2M_J$ , where  $M_J$  is Jupiter's mass. This prediction is in good agreement with the results of 3D numerical simulations (see Fig. 12).

In addition to the above viscous condition, an auxiliary condition for gap opening has been suggested based on the stability of a gap. This condition is to preclude gaps for which steep density gradients would cause an instability that prevents gap opening. This condition, called the thermal condition, is given by the requirement that the Hill radius, given by equation (2), be larger than the disk thickness,  $R_H \gtrsim H$  (Lin & Papaloizou, 1986). The critical mass for gap opening by this condition is given by

$$\frac{M_p}{M_s} \gtrsim 3 \left( \frac{H}{a} \right)^3. \quad (51)$$

For  $H/r = 0.05$ , this condition requires a larger planet mass for gap opening than equation (50) for  $\alpha \lesssim 0.01$ . A condition that combines both equations (50) and (51) has been proposed by Crida *et al.*, 2006. Even if both the thermal and viscous conditions are satisfied and  $R_H \gtrsim H$ , a substantial gas flow may occur through the gap and onto the planet (Artymowicz & Lubow, 1996; Lubow & D'Angelo, 2006).

The migration rate of a planet embedded in a gap is quite different from the Type I case that we have already considered. A planet that opens a gap in a massive disk, a disk whose mass is much greater than the planet's mass, would be expected to move inward, pushed along with the disk accretion inflow. The planet simply communicates the viscous torques across the gap by means of tidal torques that balance them. The Type II migration timescale is then of order the disk viscous timescale

$$t_{\text{vis}} \sim \frac{a^2}{\nu} \sim \frac{a^2}{\alpha cH} \sim \left( \frac{a}{H} \right)^2 \frac{1}{\alpha \Omega_p}, \quad (52)$$

which is  $\sim 10^5$  years at Jupiter's orbital radius about the Sun for  $\alpha = 0.004$ ,  $H = 0.05a$ , and  $\Omega_p = 2\pi/12 \text{ yr}^{-1}$ .

Therefore, the migration timescale can be much longer than the Type I migration timescale for higher mass planets that open gaps, as is found in simulations ( $M_p > 0.1M_J$  in Figs. 1 and 10). However, this timescale is still shorter than the observationally inferred global disk depletion timescales  $\sim 10^6 - 10^7$  years. The actual migration rate may need to be somewhat smaller, in order to explain the abundant population of observed extrasolar giant planets beyond 1AU (*Ida & Lin 2008*).

In practice, the conditions for pure Type II migration are unlikely to be satisfied. The disk mass may not be very large compared to the planet mass and the disk gap may not be fully clear of material. However, simulations have shown that to within factors of a few, the migration timescale matches the viscous timescale,  $t_{\text{vis}}$ . This result holds over a wide range of parameters, provided that the tidal clearing is substantial and the disk mass is at least comparable to the planet mass (e.g., Fig. 10).

Another way of understanding the Type II torques is to recognize that the distribution of tidal torques per unit disk mass, as seen in Fig. 11 still approximately applies, even if the disk has a deep gap that is not completely clear of material. The disk density through the gap region adjusts so that the planet migration rate is compatible with the evolution of the disk-planet system.

### 3. OUTSTANDING QUESTIONS

We describe some of the major issues involved with the theory of planet migration. The topics, descriptions, and references are by no means intended to be complete. The purpose is to introduce a few of the questions and some of the suggested solutions.

Planet migration is difficult to calculate for a variety of reasons, as described near the end of the Introduction. There are technical challenges in determining the properties of migration torques. For example, the coorbital torques are subject to saturation by nonlinear feedback effects. Lindblad torques grow in strength with proximity to the planet. Their contributions depend on the details of how the torques are limited near the planet. For the simple disk structures (e.g., moderate turbulent viscosity, fixed and smooth temperature distributions, smooth density distributions - apart from the density perturbations and gaps produced by the planet), the theory has been verified by various multi-dimensional nonlinear hydrodynamic simulations (e.g., Figs. 1, 10, and 11). But such simple disk structures may not arise in real systems. Indeed, the problems with shortness of planet migration timescales suggests that more complicated disk structures and physical processes (such as more complicated thermal effects) may be important. The disk structures influence migration, since migration torques are sensitive to gradients of disk properties. But we do not have a complete theory for these disk structures. In addition, migration depends somewhat on the detailed properties of disk turbulence that are not well understood.

#### 3.1 Limiting/Reversing Type I Migration

As seen in Fig. 1, the timescales for Type I migration, based on the model described in Section 2, are short compared to gas disk lifetimes of several million years. They become even shorter for a disk having a mass greater than the minimum mass solar nebula. As emphasized earlier, the shortness of the timescales for Type I migration is a serious problem for understanding how planets form and survive in a gaseous disk. To be consistent with the ubiquity of extrasolar gas giants and formation of Jupiter and Saturn, some studies suggest that the inward Type I migration rates must be reduced by more than a factor of 10 (*Alibert et al. 2005; Rice & Armitage 2005; Ida & Lin 2008*). One major question is whether there are processes that could slow the migration. Several ideas have been proposed. Major uncertainties about them arise due to our lack of knowledge about the detailed structure of the disks.

We briefly discuss below a few of the several suggested mechanisms for slowing Type I migration. We also discuss some processes that may reverse migration, resulting in outward migration.

The fundamental tendency for Type I to be rapid can be difficult to cancel without artificially fine tuning some other effect that provides outward torques. In general, processes that provide outward torques tend to result in either rapid inward or rapid outward migration. However, there are effects that provide an opposing torque that increases as the planet continues migrating (via feedback effects or "traps"). Such processes can naturally maintain halted migration once the inward and outward torques are in balance.

##### *Weak turbulence*

For an inwardly migrating planet, there is a dynamical feedback effect associated with the radial motion of the planet that raises the axisymmetric gas surface density within a region interior to the orbit of the planet, and lowers the density within a region exterior to the orbit (*Ward, 1997*), in the same sense as a plow operating in the radial direction. The planet pushes material away from its orbital radius as it migrates. This leads to a pile-up of material in the direction of its radial motion (see Fig. 13). The feedback then enhances the positive torques that arise in the inner disk and slows inward migration. For the feedback to exist, the effects of disk turbulence must be sufficiently weak, otherwise the density perturbations are erased by the effects of turbulent diffusion. This feedback grows with planet mass. Above some critical planet mass  $M_{\text{cr}}$ , the feedback becomes strong enough that the planet can no longer migrate. When migration is halted, the density perturbations are initially mild and there is no substantial gap (unlike the Type II migration case). There is just a sufficient density asymmetry across the orbit of the planet to change the competition between inward and outward torques away from favoring the inward torques. In subsequent evolution, the planet begins forming a gap.

The value of the critical planet mass  $M_{\text{cr}}$  depends on several factors such as how far from the planet the density perturbations occur. For disks with  $H/r \sim 0.05$  and low turbulent viscosity  $\alpha \lesssim 10^{-4}$ , the density perturbations

produced by shocked density waves in 2D disks cause migration to be sharply reduced at values of  $M_{\text{cr}} \sim 10M_{\oplus}$  (10 Earth masses) (Rafikov, 2002; Li *et al.*, 2009; see Fig. 14). For disk turbulent viscosity parameter  $\alpha \gtrsim 10^{-3}$ , Type I migration proceeds with little reduction, since the density perturbations are washed out by the effects of disk turbulence. We have little direct information on what the  $\alpha$  value should be. Some indirect evidence based on observed accretion rates onto young stars suggests that the average  $\alpha \gtrsim 10^{-4}$ . Theory suggests that there may be disk regions of low  $\alpha$  in magnetically unstable disks (the so-called dead zones of low ionization Gammie, 1996).

#### Disk Density/Temperature Variations

The torque on a planet depends somewhat on differences in properties of the disk across the planet’s orbit, as we have seen in Section 2. If the density and temperature smoothly decreases in radius at rates typically expected, the outcome is inward migration (see equation (41) and Fig. 1). We expect this to be generally true across the disk, but there could be regions where the density abruptly changes or where the radial temperature gradient is less negative or is even positive. To slow migration, the effects of these gradients would need to counteract the general trend of inward migration discussed earlier that is due to other asymmetric effects, such as the asymmetries associated with Keplerian rotation. It is possible that rapid changes in disk properties with radius could occur as a consequence of strong radial variations in disk opacity or turbulent viscosity. They can in turn modify the typically adopted gradients of density and temperature that led to our estimated migration timescales. A planet could then experience slowed migration or even be trapped with no further inward migration (e.g., Menou & Goodman, 2004; Masset *et al.*, 2006, Matsumura *et al.*, 2007). However, our current knowledge about disk structure is limited.

Disk temperature variations can also be caused by the planet itself. The planet reduces the disk thickness  $H$  of gas close to it, as a consequence of its gravity. As a result, gas close to and just outside the orbit of the planet is further exposed to the stellar radiation and experiences additional heating by the star. Gas just inside the orbit of the planet experiences some shadowing. This effect acts to decrease the temperature gradient  $\chi$  defined in equation (42). Calculations by Jang-Condell & Sasselov, 2005 have shown that this effect can reduce the Type I migration rates by up to about a factor of 2.

#### Turbulent Fluctuations

The effects of disk turbulence are typically described by means of a turbulent viscosity, e.g., equation (44). The numerical simulations used in Fig. 1 applied this model. Viscosity provides an approximate description of the dynamical effects of turbulent fluctuations that are averaged over the small space and short time scales characteristic of the turbulence. But, the time-dependent, small-scale density fluctuations can give rise to fluctuating random torques on the planet that are not described by viscosity. Unlike the Type I torque that acts continuously in the same di-

rection, the fluctuating torque undergoes changes in direction on timescales characteristic of the turbulence that are short compared with the migration timescale. The fluctuating torque causes the planet to undergo something like a random walk. For the effects of the random walk to completely dominate over Type I migration, the amplitude of the fluctuating torque must be much larger than the Type I torque that acts steadily.

The change in the angular momentum of the planet due to a random torque  $T_{\text{R}}$  over some time  $t$  is given by  $\sim \sqrt{N}T_{\text{R}}t_{\text{R}}$ , where  $N = t/t_{\text{R}}$  is the number of fluctuations felt by the planet and  $t_{\text{R}}$  is the characteristic timescale for the torque fluctuation, perhaps of order the orbital period. The planet experiences many torque fluctuations over the migration timescale,  $N \gg 1$ . The change in the planet angular momentum by the Type I torque  $T$  is given by  $\sim Tt$ . For random torques to dominate, we require  $T_{\text{R}} \gtrsim \sqrt{N}T$ . We take  $t$  to be the Type I timescale of  $\sim 10^5$  yr and  $t_{\text{R}} \sim 10$  yr, so that  $N \sim 10^4$  and we require  $T_{\text{R}}$  to be  $\gtrsim 100T$ . Torque  $T_{\text{R}}$  depends linearly on the planet mass, while the Type I torque  $T$  increases quadratically with the planet mass and the Type I migration time  $t$  decreases with the inverse of the planet mass. Therefore, the random torque is then more important for lower mass planets. The nature of the random torque depends on the properties of the disk turbulence, in particular the amplitude  $T_{\text{R}}$  and correlation timescale  $t_{\text{R}}$  for the fluctuating torques, which are currently not well determined.

Some global simulations and analytic models suggest that turbulent fluctuations arising from a magnetic instability (the magneto-rotational instability Balbus & Hawley, 1991) are important for migration of lower mass planets (Nelson, 2005; Johnson *et al.*, 2006; see Fig. 15). Some other simulations, those done for a small region of the disk called “box” simulations, suggest that these fluctuating torques are not effective enough to play an important role in planet migration (Yang *et al.*, 2009). Both the global and box simulations are very computationally demanding and the current results cannot be regarded as definitive. The box simulations have higher resolution than the global ones, since they cover a smaller region. However, they may miss important effects, if they occur on larger scales than the box size. The direct global simulations, such as those in Fig. 15, cover much less time than the Type I migration timescale for a low mass planet and consequently may not reveal the competing effects of unidirectional Type I torques.

Unlike Type I migration, the survival of a planet within a disk where fluctuating torques dominate is described statistically. Over time, there is a smaller probability that planets survive in the disk. But there is always a nonzero probability of survival.

However, if turbulent fluctuations are important for migration, then the eccentricities of planetesimals are pumped up so highly that collisions between them may result in their destruction rather than accretion (Ida *et al.*, 2008). Therefore, although the turbulent fluctuations may inhibit the infall of planetary cores into the central star by migration,

they may inhibit the build up of the cores necessary for giant planet formation in the core accretion model.

#### *Ordered Magnetic Field*

An ordered magnetic field can affect the nature of disk-planet interactions. *Terquem*, 2003 analyzed the effects of an ordered (nonrandom) toroidal magnetic field on Type I planet migration. The magnetic field introduces additional resonances, called magnetic resonances, that lie closer to the planet than the Lindblad resonances, whose locations are given by equation (38). As a result, the magnetic resonances can be stronger than the Lindblad ones. As in the case of the Lindblad resonances, a magnetic resonance located interior (exterior) to the orbit of the planet causes outward (inward) planet migration. If the magnetic field strength falls off sufficiently fast with distance from the star, the inner magnetic resonance dominates, and slowed or even outward migration can occur. For example, in the case that the magnetic energy density is comparable to the gas thermal energy density in the disk, an outward torque on the planet can be produced, if the magnetic-to-gas energy density ratio falls off faster than  $r^{-2}$ . How this ratio varies within a disk is not known, although such a variation is quite plausible in some situations. If the magnetic field is responsible for the disk turbulence, then the toroidal field would contain a fluctuating component that complicates the outcome.

#### *Migration Driven By Nonisothermal Effects in the Coorbital Region*

The disk is heated by the central star and by viscous turbulent dissipation. Many studies of disk-planet interactions simplify the disk temperature structure to be locally isothermal. In this approximation the temperature distribution depends on radius in a fixed, prescribed manner. Such a situation can arise if the optical depth of the disk is low enough that it efficiently radiates any excess energy due to compression caused by interactions with the planet. The locally isothermal assumption is frequently applied in numerical simulations and was applied in obtaining equation (41). The behavior in the isothermal limit tends to suggest that coorbital torques do not typically dominate migration (e.g., equation (41)).

But, recent work has suggested that nonisothermal behavior could have an important effect on coorbital torques and the overall planet migration rate. The nonisothermal regime has been explored in simulations by *Paardekooper & Mellema*, 2006 who found that slowed and even outward migration due to coorbital torques may occur in certain regimes. Recent studies have suggested that a background radial entropy gradient could play a role in determining the corotational torque if the gas undergoes adiabatic changes in its interactions with the planet. This effect may provide an additional contribution to the coorbital torque beyond the vortensity gradient that appears in equation (35). The slowing/reversing of migration appears to involve the conditions that the disk have a negative radial entropy gradient, sufficient viscosity to avoid coorbital torque saturation, and a thermal timescale that is long enough for the gas to behave

adiabatically as it passes the planet. The nature of this effect and the conditions required for it to operate is an active area of investigation (e.g., *Baruteau & Masset*, 2008).

### **3.2 Other Migration Processes Involving a Gaseous Disk**

#### *Runaway Coorbital Migration, Type III Migration*

The coorbital torque will be saturated (reduced to zero) unless some effect is introduced to break the symmetry of the streamlines, such as turbulent viscosity (see discussion in Section 2.2). However, planet migration itself introduces an asymmetry and could therefore act to prevent torque saturation. (The coorbital torque model presented in Section 2.3 ignored the effects of planet migration on the horseshoe orbits in Fig. 2.) The coorbital torque for a migrating planet could then depend on the rate of migration. Under some conditions, the coorbital torque could in turn cause faster migration and in turn a stronger torque, resulting in an instability and a fast mode of migration (*Masset & Papaloizou*, 2003). The resulting migration is sometimes referred to as Type III migration. To see how this might operate in more detail, we consider the evolution of gas trapped in the coorbital region (*Artymowicz*, 2004; *Ogilvie & Lubow*, 2006). For a sufficiently fast migrating planet, the topology of the streamlines changes with open streamlines flowing past the planet and closed streamlines containing trapped gas (see Fig. 16). The leading side of the planet contains trapped gas acquired at larger radii, while the gas on the trailing side is ambient material at the local disk density. The density contrast between material on the trailing and leading sides of the planet gives rise to a potentially strong torque. The migration timescales are of order the Type I migration timescales. This timescale can be very short for planets that are massive enough to partially open a gap and would otherwise not undergo Type I migration. The migration timescales have been found to be as short as 10-20 orbits in the case of a Saturn mass planet embedded in a cold and massive disk. A major question centers around the conditions required for this form of migration to be effective and therefore whether planets typically undergo such migration.

#### *Migration of Eccentric Orbit Planets*

The analysis of migration in Section 2 assumed that planets reside on circular orbits. This assumption is not unreasonable, since there are strong damping effects on eccentricity for a planet that does not open a gap in the disk (*Artymowicz*, 1993). Some eccentricity may be continuously produced by turbulent fluctuations in the gas, as described above, or by interactions with other planets. In general, eccentricity damping is faster than Type I migration. For planets that open a gap, it is possible that they reside on eccentric orbits in the presence of the gaseous disk. In fact, one model for the observed orbital eccentricities of extra-solar planets attributes the excitation of eccentricities to disk-planet interactions (*Goldreich & Sari*, 2003; *Ogilvie & Lubow*, 2003).

A planet on a sufficiently eccentric orbit embedded in a

circular disk can orbit more slowly at apoastron than the exterior gas with which it tidally interacts. Similarly, a planet can orbit more rapidly than the tidally interacting gas at periastron. These angular velocity differences can change the nature of the "friction" between the planet and the disk discussed in Section 2.2. For example, at apoastron the more slowly orbiting planet could gain angular momentum from the more rapidly rotating nearby gas that lies outside its orbit. Furthermore, since the planet spends more time at apoastron than periastron, the effects at apoastron could dominate over effects at periastron. It is then possible that outward migration could occur for eccentric orbit planets undergoing Type I migration, assuming such planets could maintain their eccentricities (Papaloizou, 2002).

In the case of a planet that opens a gap, simulations suggest that slowed or even outward migration may occur as the planet gains eccentricity from disk-planet interactions (D'Angelo *et al*, 2006). The situation is complicated by the fact that the gaseous disk can gain eccentricity from the planet by a tidal instability (Lubow, 1991). For the outward torque to be effective, there needs to be a sufficient difference in the magnitude and/or orientation between the planet and disk eccentricities, so that the planet moves slower than nearby disk gas at apoastron.

#### *Multiplanet Migration*

Thus far, we have only considered single planet systems. Of the more than 200 planetary systems detected to date by Doppler techniques, over 10% are found in multi-planet systems (Butler *et al*, 2006). Systems have been found to have orbits that lie in mutual resonance, typically the 2:1 resonance. The resonant configurations are likely to be the result of convergent migration, migration in which the separation of the orbital radii decreases in time. This process occurs as the outer planet migrates inward faster than the inner planet. Planets can become locked into resonant configurations and migrate together, maintaining the planetary orbital frequency ratio of the resonance (see also Chapter 10). The locking can be thought of as a result of trapping the planets within a well of finite depth. Just which resonance the planets become locked into depends on their eccentricities and the relative rate of migration that would occur if they migrated independently. As planets that are initially well-separated come closer together, they lock into the first resonance that provides a deep enough potential to trap them against the effects of their convergence. We discuss below some consequences of resonant migration.

To maintain a circular orbit, a migrating planet must experience energy,  $E$ , and angular momentum,  $J$ , changes that satisfy  $\dot{E} = \Omega_p \dot{J}$ , where the angular speed of the planet  $\Omega_p$  varies as the planet migrates. As the planets migrate together in a resonant configuration, their mutual interactions cause deviations from this relation. As a result, their energies and angular momenta evolve in a way that is incompatible with maintaining a circular orbit. Substantial orbital eccentricities can develop as a consequence of migration (Yu & Tremaine, 2001; Lee & Peale, 2002). In addition, migration can cause a large amplification of an initially

small mutual inclination of the planetary orbit planes (Yu & Tremaine, 2001; Thommes & Lissauer, 2003; see Fig. 17).

Planetary system GJ876 is a well-studied case in which the planets are in a 2:1 resonance. If the system's measured eccentricities are due to resonant migration, then according to theory (Lee & Peale, 2002), the system migrated inward by less than 10%. Such a small amount of locked migration seems unlikely. It is more reasonable to expect that some process limited further eccentricity growth. Disk-planet interactions could have limited the eccentricities and inclinations that could be developed by resonant migration. For a single planet interacting with a disk, theory and simulations suggest that eccentricity is generally damped for planets of low mass, too low to open a gap. A higher mass (gap opening) planet can undergo eccentricity growth due to its interaction with the disk. But the level of eccentricity produced is limited and eccentricity damping occurs above that level (D'Angelo *et al*, 2006). The disk-planet mutual inclination can also be suppressed or limited by the dissipation of disk warps (Lubow & Ogilvie, 2001). Recent simulations suggest that disk-planet interactions due to gas interior to the orbit of the inner planet could have limited the eccentricities of multi-planet systems to observed levels (Crida *et al*, 2008). But it may be possible under certain circumstances, such as a depleted inner disk, that large eccentricities and orbital inclinations could develop due to such processes.

### 3.3 Other Forms of Migration

#### *Migration in a Planetesimal Disk*

After the gaseous disk is cleared from the vicinity of the star, after about  $10^7 y$ , there remains a disk of solid material in the form of low mass planetesimals. This disk is of much lower mass than the original gaseous disk. But the disk is believed to have caused some migration in the early solar system with important consequences (Hahn & Malhotra, 1999; Tsiganis *et al*, 2005).

There is strong evidence that Neptune migrated outward. This evidence comes from observations of Kuiper belt objects that are resonantly trapped exterior, but not interior, to Neptune's orbit. The detailed dynamics of a planetesimal disk are somewhat different from the case of a gaseous disk, as considered in Section 2. The planetesimals behave as a nearly collisionless system of particles. Jupiter is much more massive than the other planets and can easily absorb angular momentum changes in Neptune. As Neptune scatters planetesimals inward and outward, it undergoes angular momentum changes. It is the presence of Jupiter that breaks the symmetry in Neptune's angular momentum changes. Once an inward scattered planetesimal reaches the orbit of Jupiter, it gets flung out with considerable energy and does not interact again with Neptune. As a result of the loss of inward scattered particles, Neptune gains angular momentum and migrates outward, while Jupiter loses angular momentum and migrates slightly inward.

A somewhat analogous process occurs in gaseous circumbinary disks, disks that orbit around binary star systems



(Pringle, 1991). The circumbinary disk gains angular momentum at the expense of the binary. The binary orbit contracts as the disk outwardly expands. A gap-opening planet embedded in a circumbinary disk (or under some conditions, a disk that surrounds a star and massive inner planet) would undergo a form of Type II migration that could carry the planet outward (Martin *et al.*, 2007). In the solar system case, the Sun-Jupiter system plays the role of the binary. Viscous torques are the agent for transferring the angular momentum from the binary outward in the gaseous circumbinary disk, while particle torques play the somewhat analogous role in the planetesimal disk.

In a planetesimal disk, another process can operate to cause migration. This process is similar to the runaway coorbital migration (Type III migration) described above, but applied to a collisionless system of particles (Ida *et al.* 2000). Interactions between the planetesimals and the planet in the planet’s coorbital zone can give rise to a migration instability.

#### Kozai Migration

A planet that orbits a star in a binary star system can periodically undergo a temporary large increase in its orbital eccentricity through the a process known as the Kozai effect (see also Chapter 10). Similar Kozai cycles can occur in multi-giant planet systems. The basic idea behind Kozai migration is that the increased eccentricity brings the planet closer to the star where it loses orbital energy through tidal dissipation. In the process, the planet’s semi-major axis is reduced and inward migration occurs (Wu & Murray, 2003). We describe this in more detail below.

Consider a planet in a low eccentricity orbit that is well interior to the binary orbit and is initially highly inclined with respect to it. The orbital plane of the planet can be shown to undergo tilt oscillations on timescale of  $\sim P_b^2/P_p$ , where  $P_b$  is the binary orbital period,  $P_p$  is the planet’s orbital period, and by assumption  $P_b \gg P_p$ . Under such conditions, it can be shown that the component of the planet’s angular momentum perpendicular to the binary orbit plane (the  $z$ -component) is approximately conserved,  $J_z = M_p \sqrt{GM_s a_p (1 - e_p^2)} \cos I$ , where  $a_p$  and  $e_p$  are respectively the semi-major axis and eccentricity of the planet’s orbit and  $I$  is the inclination of the orbit with respect to the plane of the binary.

The conservation of  $J_z$  is easily seen in the case that the binary orbit is circular and the companion star is of low mass compared to the mass of the star about which the planet orbits. On such long timescales  $\gg P_b$ , the companion star can be considered to be a continuous ring that provides a static potential. In that case, the azimuthal symmetry of the binary potential guarantees that  $J_z$  is conserved. By assumption, we have  $\cos I \ll 1$  and  $e_p \ll 1$  in the initial state of the system. As the planet’s orbital plane evolves and passes into alignment with the binary orbital plane,  $\cos I \sim 1$ , conservation of  $J_z$  requires  $e_p \sim 1$ . In other words,  $J_z$  is initially small because of the high inclination of the orbit. When the inclination drops, the orbit must be-

come more eccentric (radial), in order to maintain the same small  $J_z$  value. The process then periodically trades high inclination for high eccentricity.

During the times of increased eccentricity, the planet may undergo a close encounter with the central star at periastron distance  $a_p(1 - e_p)$ . During the encounter, the tidal dissipation involving the star and planet results in an energy loss in the orbit of the planet and therefore a decrease in  $a_p$ . This process then results in inward planet migration. The energy loss may occur over several oscillations of the orbit plane.

Another requirement for the Kozai process to operate is that the system must be fairly clean of other bodies. The presence of another object could induce a precession that washes out the Kozai effect. Given the special requirements needed for this process to operate, it is not considered to be the most common form of migration. However, there is good evidence that it does operate in some systems (Takeda & Rasio, 2005). The Kozai effect can also occur in two-planet systems, where the outer planet plays the role of the binary companion. The process can be robust due to the proximity of outer planet (Nagasawa *et al.* 2008).

### 3.4 Techniques Used in Numerical Simulations

Numerical simulations provide an important tool for analyzing planet migration. They can provide important insights in cases where nonlinear and time-dependent effects are difficult to analyze by analytic methods. Simulations, as well as analytical models, depend on a model of appropriate physical processes, such as heating and cooling, the treatment of the disk turbulence (either by a viscosity or detailed modeling of the disk instability that causes the turbulence), and the model of the disk structure. Below we discuss some issues related to the use of simulations for simple (isothermal and alpha-disk) multi-dimensional models of disk-planet interactions.

Some powerful grid-based hydrodynamics codes (such as the ZEUS code Stone & Norman, 1992) have been adapted to the study of disk-planet interactions. In addition, particle codes based on the Smoothed Particle Hydrodynamics (SPH) (Monaghan, 1992) have sometimes been employed. A systematic comparison between many of the codes has been carried out by de Val-Borro *et al.*, 2006. We discuss a few basic points. For planets that open a gap, grid-based codes offer an advantage over particle-based codes. The reason is that the resolution of grid based codes is determined by the grid spacing, while the resolution of particle-based codes is determined by the particle density. If a planet opens an imperfect gap, the particle density and resolution near the planet is low. Higher resolution occurs where the particle density is higher. On the other hand, SPH well represents regions of a cold disk that are away from a planet. The gas follows the trajectories of SPH particles that are slightly modified by gas pressure and tidal forces. SPH provides high resolution in dense regions, such as near the cores of low mass planets embedded in disks (Ayliffe &

Bate, 2007).

There have been variable resolution techniques developed for grid-based codes in which the highest resolution is provided in regions near the planet where it is needed, such as nested grid methods (D'Angelo *et al.*, 2002). Such techniques need to provide a means of joining the regions of high and low resolution without introducing artifacts (such as wave reflections) or lowering the overall accuracy of the scheme.

Grid-based codes that simulate disk-planet interactions typically employ numerical devices to improve convergence. For example, the gravitational potential of the planet is often replaced by one that does not diverge near the planet. The potential is limited by introducing a smoothing length, a distance within which the potential does not increase near the planet. Another limitation is that the simulated domain of the disk is typically limited to a region much smaller than the full extent of the disk. Techniques have been developed to ensure that reflections from the boundaries do not occur, e.g., by introducing enhanced wave dissipation near the boundary or approximate outgoing wave boundary conditions.

The time-steps of codes are limited by the Courant condition. Short time-steps often result from the region near the inner boundary of the computational domain (smaller radii) where the disk rotation is fastest. As a result, it is difficult to extend the disk very close to the central star. The FARGO scheme (Masset, 2000) is very useful in overcoming this limitation. However, the method is difficult to apply to a variable grid spaced code.

Convergence is a major issue with these simulations. Ideally, one should demonstrate that the results of the simulations are sufficiently insensitive to the locations of the boundaries, the size of the smoothing length, the size of the time steps, and the grid resolution. Even the direction of migration can be affected by the size of the potential smoothing length in certain cases. In a 2D simulation, a finite smoothing length  $\sim H$  provides a means of simulating the reduced effects of planet gravity on a disk of finite thickness. But in the 2D case, the limit of zero smoothing length is unphysical. In practice, testing for convergence is computationally expensive, but can be done for a subset of the models of interest, perhaps over a limited time range. Demonstrating convergence is important for providing reliable results.

#### 4. FUTURE PROSPECTS

The theory of planet migration is intertwined with the theory of planet formation (Chapter 13). The timescale for a planet to grow within a disk is a key element in understanding whether planet migration is a major obstacle to planet formation. We have pointed out that the formation timescales for gas giant planets in the core accretion model do present a problem for the simplest planet migration theories. However, alternative migration models, some of which

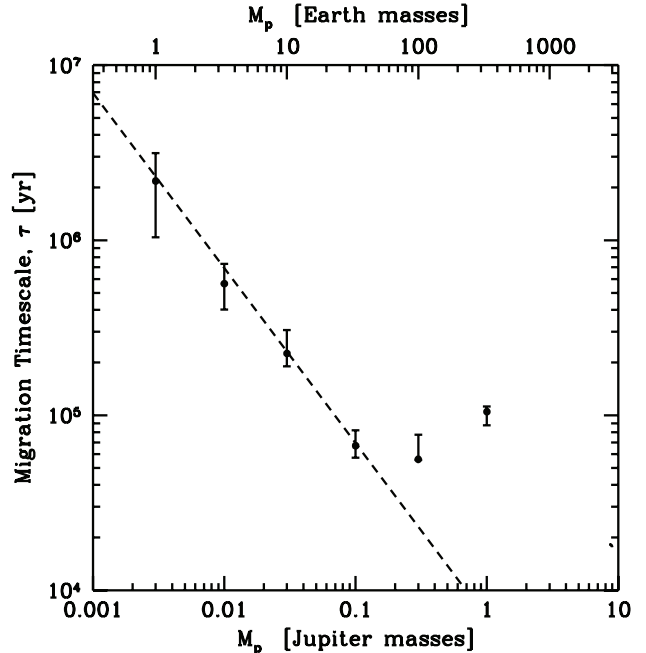


Fig. 1.— Migration timescales versus planet mass for a planet embedded in a 3D disk of mass  $\sim 0.02M_s$  with surface density  $\Sigma \propto r^{-1/2}$  and  $H/r = 0.05$ . The planets are on fixed circular orbits and have fixed masses and orbit a solar mass star. The dots with error bars denote results of 3D numerical simulations with the same disk parameters (Bate *et al.*, 2003). The dashed line plots equation (41) based on linear theory (Tanaka *et al.*, 2002). Above about  $0.1M_J$ , the planet opens a gap in the disk, Type I theory becomes invalid, and Type II migration occurs.

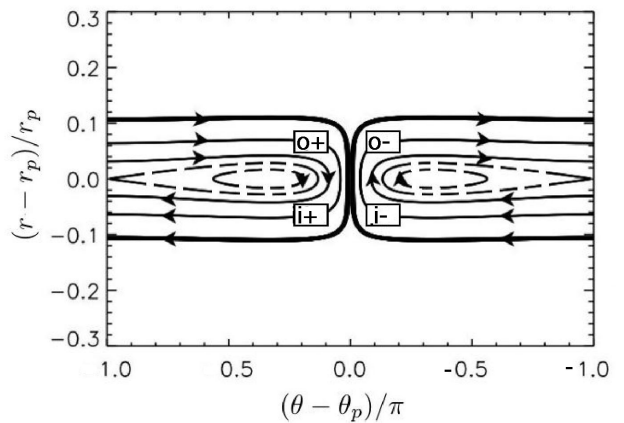


Fig. 2.— Coorbital streamlines near a Saturn mass planet that orbits a solar mass star,  $M_p = 3 \times 10^{-4} M_s$ . The origin is centered on the planet and corotates with it. Azimuthal angle  $\theta$  about the star increases to the left. The outermost streamlines are at the edge of the coorbital region. Solid streamlines are the horseshoe orbits. Locations  $i\mp$  and  $o\mp$  label the positions near the encounter with the planet.

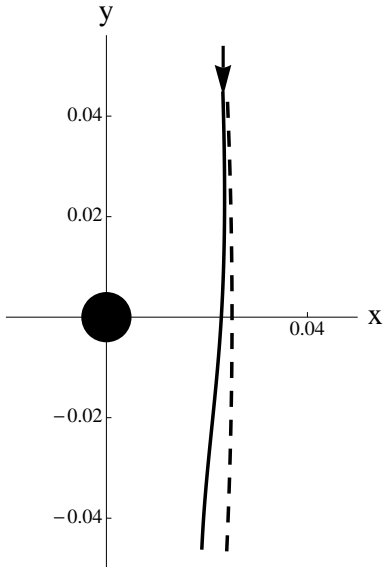


Fig. 3.— Path of a particle that passes by a planet of mass  $M_p = 10^{-6} M_s$  (0.3 Earth masses for a planet that orbits a solar mass star). The coordinates are in units of the orbital radius of the planet  $a$ . The planet lies at the origin, while the star lies at  $(-1, 0)$ . The dashed line follows the path that is undisturbed by the planet with  $x = 0.025a$ , while the solid line follows the path resulting from the interaction with the planet. In the frame of the planet, the particle moves in the negative  $y$  direction.

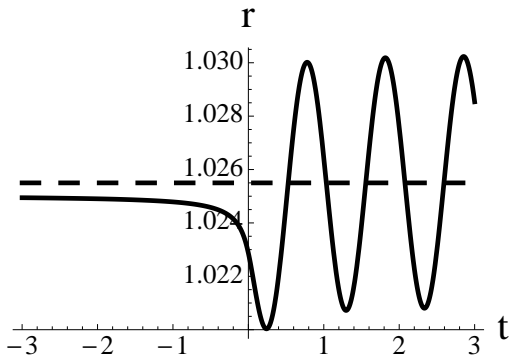


Fig. 4.— The solid line plots the particle distance from the star  $r$  in units of  $a$  as a function of time in units of planet orbit periods for the particle that follows the perturbed path in Fig. 3. The particle passes the planet at time  $t = 0$ . Immediately after passage by the planet, the particle is deflected toward smaller radii, toward the planet, and acquires an eccentricity, as indicated by the radial oscillations. The dashed line plots the mean radius of these oscillations. Since the mean radius of the oscillations is larger than the initial orbital radius (compare dashed line with solid line at  $t < -1$ ), the particle gained energy and angular momentum, as a consequence of its interaction with the planet.

are described in Section 3, may be appropriate. Future prospects for resolving this issue depend on advances in the theory of planet formation.

Prospects for making progress in the theory of planet migration rely on including and more accurately representing physical processes in the models, improving computer simulations, and obtaining a better understanding of the structure of planet-forming gaseous disks.

Planet migration in disks is a consequence of the action of Lindblad and corotational resonances, as described in Section 2. The theory of Lindblad resonances is better understood. Their linear and nonlinear properties have been analyzed in more detail. The corotational resonances are somewhat more delicate and less well understood. Progress on the theory of planet migration will likely involve further investigations of the role of corotational resonances (e.g., *Paardekooper & Mellema, 2006*).

Improvements to computer capabilities and codes should allow simulations to be carried out with higher resolution over longer timescales. Progress will be made by also including more physical effects. For example, most multi-dimensional simulations have made only the simplest assumptions about the thermal properties of the disk. The use of a turbulent viscosity is a serious approximation to the effects of turbulence. Directly simulating the instability that produces the turbulence along with planet migration is a major computational challenge (e.g., *Nelson, 2005*).

Some calculations have suggested that higher mass eccentric orbit planets could undergo slowed or outward migration due to their interactions with a gaseous disk. But we do not know whether such planets have acquired their eccentricities at this early stage. Observations of the eccentricities young planets would be quite valuable in understanding this issue. It would be useful to know whether planetary eccentricities are determined at early times, suggesting that planet eccentricities are present while the planet is embedded in its gaseous disk.

A major uncertainty in the theory of planet migration is the physical state of the disk. Low mass planet migration behaves very differently depending on the level of disk turbulence and the structural properties of the disk (Section 3). For example, in weakly turbulent disks, feedback effects may halt Type I migration. While in highly turbulent disks, fluctuating torques may dominate over Type I torques. The presence of rapid radial density variations or weakened (or inverted) radial temperature variations can substantially alter migration, since it depends on the competition between torques involving material just inside and outside the orbit of the planet. The better determination of disk properties will likely rely on some combination of improved theory and observations. It is unlikely that theory alone will be able to make much progress along these lines because, for example, the density structure depends on the disk turbulence that is difficult to accurately predict from first principles. Once such difficulty is that magnetically driven turbulence is strongly affected by the abundance and size distribution of dust grains that control the level of disk ionization

(e.g., *Salmeron & Wardle, 2008*). The observational determination of disk properties (disk density and temperature as a function of distance from the star) in the inner parts of protostellar disks, where planet formation is expected to occur, is important for such purposes. New telescopes such as ALMA and JWST may be quite valuable in making such determinations.

**Acknowledgments.** This work was partially supported by NASA grant NNX07AI72G to SL. We thank Phil Armitage, Gennaro D’Angelo and Jim Pringle for carefully reading a draft and suggesting improvements. We thank an anonymous reviewer for many helpful suggestions. We also benefited considerably by discussions at the Cambridge University Isaac Newton Institute Program ”Dynamics of Discs and Planets.”

## REFERENCES

- Alibert, Y., Mousis, O., Mordasini, C. and Benz, W. (2005) New Jupiter and Saturn Formation Models Meet Observations. *Astrophys. J.*, 626, L57-L60.
- Armitage, P. J., Livio, M., & Pringle, J. E. (2001), *Mon. Not. Roy. Astr. Soc.*, 324, 705-711.
- Artymowicz, P. (1993) Disk-Satellite Interaction via Density Waves and the Eccentricity Evolution of Bodies Embedded in Disks. *Astrophys. J.*, 419, 166-180.
- Artymowicz, P. and Lubow, S. H. (1996) Mass flow through gaps in circumbinary disks. *Astrophys. J.*, 467, L77.
- Artymowicz, P. (2004) Migration Type III. *KITP Conference on Planet Formation*, [http://online.kitp.ucsb.edu/online/planetf\\_c04](http://online.kitp.ucsb.edu/online/planetf_c04)
- Ayliffe, B. A. and Bate, M. R. (2009) Gas accretion on to planetary cores: three-dimensional self-gravitating radiation hydrodynamical calculations. *Mon. Not. Roy. Astr. Soc.*, 393, 49-64.
- Balbus, S. A., and Hawley, J. F. (1991) A powerful local shear instability in weakly magnetized disks. I. Linear analysis. *Astrophys. J.*, 376, 214-222.
- Baruteau, C. and Masset, F. (2008) On the Corotation Torque in a Radiatively Inefficient Disk. *Astrophys. J.*, 672, 1054-1067.
- Bate, M. R., Lubow, S. H., Ogilvie, G. I., and Miller, K. A. (2003) Three-dimensional calculations of high- and low-mass planets embedded in protoplanetary discs. *Mon. Not. Roy. Astr. Soc.*, 341, 213-229.
- Bodenheimer, P., Hubickyj, O., and Lissauer, J. J. (2000) Models of the in Situ Formation of Detected Extrasolar Giant Planets. *Icarus*, 143, 2.
- Butler, R. P., et al. (2006) Catalog of Nearby Exoplanet. *Astrophys. J.*, 646, 505-522.
- Crida, A., Morbidelli, A., and Masset, F. (2006), On the width and shape of gaps in protoplanetary disks. *Icarus*, 181, 587.
- Crida, A., Sándor, Z., & Kley, W. (2008), Influence of an inner disc on the orbital evolution of massive planets migrating in resonance, *Astron. Astrophys.*, 483, 325-337.
- Cuzzi, J. N., and Weidenschilling, S. J. (2006), Particle-Gas Dynamics and Primary Accretion, in *Meteorites and the Early Solar System II*, (Lauretta & McSween Jr. eds.), Univ. Arizona Press, Tucson.
- D’Angelo, G., Henning, T., and Kley, W. (2002) Nested-grid calculations of disk-planet interaction. *Astron. Astrophys.*, 385, 647-670.
- D’Angelo, G., Lubow, S. H., and Bate, M. R. (2006) Evolution of Giant Planets in Eccentric Disks. *Astrophys. J.*, 652, 1698-1714.
- D’Angelo, G., and Lubow, S. H. (2008) Evolution of Migrating Planets Undergoing Gas Accretion. *Astrophys. J.*, 685, 560-583.
- Gammie, C. F. (1996) Layered accretion in T Tauri disks. *Astrophys. J.*, 457, 355362.
- Goldreich, P., and Tremaine, S. (1979) The Excitation of Density Waves At the Lindblad and Corotation Resonances By an External Potential *Astrophys. J.*, 233, 857-871.
- Goldreich, P., and Tremaine, S. (1980) Disk-satellite interactions. *Astrophys. J.*, 241, 425-441.
- Goldreich, P., and Tremaine, S. (1982) The Dynamics of Planetary Rings. *Ann. Rev. Astron. Astrophys.*, 20, 249-283.
- Goldreich, P., and Sari, R. (2003) Eccentricity Evolution For Planets in Gaseous Disks. *Astrophys. J.*, 585, 10241037.
- Hahn, J. M., & Malhotra, R. (1999) Orbital Evolution of Planets Embedded in a Planetesimal Disk. *Astron. J.*, 117, 3041-3053.
- Hayashi, C. (1981) Structure of the solar nebula, growth and decay of magnetic elds and effects of magnetic and turbulent viscosities on the nebula. *Progress of Theoretical Physics Supplement*, 70, 3553.
- Hourigan, K. & Ward, W. R. (1984) Radial Migration of Preplanetary Material: Implications for the Accretion Time Scale Problem, *Icarus*, 60, 29-39.
- Ida, S., Bryden, G., Lin, D. N. C. and Tanaka, H. (2000) Orbital migration of Neptune and orbital distribution of trans-Neptunian objects. *Astrophys. J.*, 534, 428-445.
- Ida, S., and Lin, D. N. C. (2004) Toward a deterministic model of planetary formation. I. A desert in the mass and semimajor axis distributions of extrasolar planets. *Astrophys. J.*, 604, 388-413.
- Ida, S., Guillot, T., and Morbidelli, A. (2008) Accretion and destruction of planetesimals in turbulent disks. *Astrophys. J.*, 686, 1292-1301.
- Ida, S., and Lin, D. N. C. (2008) Toward a deterministic model of planetary formation. IV. Effects of type I migration. *Astrophys. J.*, 673, 487-501.
- Jang-Condell, H., and Sasselov, D. D. (2005) Type I Planet Migration in a Nonisothermal Disk. *Astrophys. J.*, 619, 11231131.
- Johnson, E. T., Goodman, J., and Menou, K. (2006) Diffusive Migration of Low-Mass Protoplanets in Turbulent Disks. *Astrophys. J.*, 647, 1413-1425.
- Lee, M. H., and Peale, S. J. (2002) Dynamics and Origin of the 2:1 Orbital Resonances of the GJ 876 Planets. *Astrophys. J.*, 567, 596-609.
- Li, H., Lubow, S. H., Li, S., and Lin, D. N. C. (2009) Type I Planet Migration in Nearly Laminar Disks. *Astrophys. J.*, 690, L52.
- Lin, D. N. C., and Papaloizou, J. (1979) Tidal torques on accretion discs in binary systems with extreme mass ratios. *Mon. Not. Roy. Astr. Soc.*, 186, 799-812.
- Lin, D. N. C., and Papaloizou, J. C. B. (1986) On the tidal interaction between protoplanets and the protoplanetary disk. III - Orbital migration of protoplanets. *Astrophys. J.*, 309, 846-857.
- Lubow, S. H. (1991) A model for tidally driven eccentric instabilities in fluid disks. *Astrophys. J.*, 381, 259-267.
- Lubow, S. H. and Ogilvie, G. I. (2001) Secular Interactions Between Inclined Planets and a Gaseous Disk. *Astrophys. J.*, 560, 997-1009.
- Lubow, S. H. and D’Angelo, G. (2006) Gas Flow Across Gaps in Protoplanetary Disks. *Astrophys. J.*, 641, 526.
- Lynden-Bell, D. and Pringle, J. E. (1974) The Evolution of Vis-

- cous Disks and the Origin of the Nebular Variables. *Mon. Not. Roy. Astr. Soc.*, 168, 603-637.
- Martin, R. G., Lubow, S. H., Pringle, J. E., & Wyatt, M. C. (2007) Planetary migration to large radii. *Mon. Not. Roy. Astr. Soc.*, 378, 1589-1600.
- Masset, F. S. (2000) FARGO: A fast eulerian transport algorithm for differentially rotating disks. *Astron. Astrophys. Supp.*, 141, 165-173.
- Masset, F. S., and Papaloizou, J. C.B. (2003) Runaway migration and the formation of hot Jupiters. *Astrophys. J.*, 588, 494508.
- Masset, F. S., Morbidelli, A., Crida, A., and Ferreira, J. (2006) Disk surface density transitions as protoplanet traps. *Astrophys. J.*, 642, 478-487.
- Matsumura, S., Pudritz, R. E. and Thommes, E. W. (2007) Saving Planetary Systems: Dead Zones and Planetary Migration. *Astrophys. J.*, 660, 1609-1623.
- Mayor, M., and Queloz, D. (1995) A Jupiter-mass companion to a solar-type star. *Nature*, 378, 355-359.
- Menou, K., and Goodman, J. (2004) Low-Mass Protoplanet Migration in T Tauri Disks. *Astrophys. J.*, 606, 520-531.
- Monaghan, J. J. (1992) Smoothed particle hydrodynamics. *Ann. Rev. Astron. Astroph.*, 30, 543-574.
- Nagasawa, M., Ida, S., and Bessho, T. (2008) Formation of hot planets by a combination of planet scattering, tidal circularization, and the Kozai mechanism. *Astrophys. J.*, 678, 498-508.
- Nelson, R. P. (2005) On the orbital evolution of low mass protoplanets in turbulent, magnetised disks. *Astron. Astrophys.* 443, 1067-1085.
- Ogilvie, G. I., and Lubow, S. H. (2003) Saturation of the Corotation Resonance in a Gaseous Disk. *Astrophys. J.*, 587, 398-406.
- Ogilvie, G. I., and Lubow, S. H. (2006) The effect of planetary migration on the corotation resonance. *Mon. Not. Roy. Astr. Soc.*, 370, 784-798.
- Paczynski, B. (1978) A model of selfgravitating accretion disk. *Acta Astronomica*, 28, 91
- Paardekooper, S.-J., and Mellema, G. (2006) Halting type I planet migration in non-isothermal disks. *Astron. Astrophys.* 459, L17-L20.
- Papaloizou, J. C. B. (2002) Global  $m = 1$  modes and migration of protoplanetary cores in eccentric protoplanetary discs. *Astron. Astrophys.* 388, 615-631.
- Pringle, J. E. (1991) The properties of external accretion discs. *Mon. Not. Roy. Astr. Soc.*, 248, 754-759.
- Rafikov, R. R. (2002) Planet Migration and Gap Formation by Tidally Induced Shocks. *Astrophys. J.*, 572, 566-579.
- Rice, W. K. M and Armitage, P. J. (2005) Quantifying Orbital Migration From Exoplanet Statistics and Host Metallicities. *Astrophys. J.*, 630, 1107-1113.
- Stone, J. M., and Norman, M. L. (2002) ZEUS-2D: A radiation magnetohydrodynamics code for astrophysical flows in two space dimensions. I - The hydrodynamic algorithms and tests. *Astrophys. J. Supp.*, 80, 753-790.
- Salmeron, R., and Wardle, M. (2008) Magnetorotational instability in protoplanetary discs: the effect of dust grains. *Mon. Not. Roy. Astr. Soc.*, 388, 1223-1238.
- Shakura N. I., and Sunyaev R. A., (1973), Black holes in binary systems. Observational appearance. *Astron. Astrophys.* 24, 337 - 355.
- Takeda, G., and Rasio, F. A. (2005) High Orbital Eccentricities of Extrasolar Planets Induced by the Kozai Mechanism. *Astrophys. J.*, 627, 1001-1010.
- Tanaka, H., Takeuchi, T., & Ward, W. R. (2002) Three-Dimensional Interaction between a Planet and an Isothermal Gaseous Disk. I. Corotation and Lindblad Torques and Planet Migration. *Astrophys. J.*, 565, 1257-1274.
- Terquem, C. E. J. M. L. J. (2003) Stopping inward planetary migration by a toroidal magnetic field. *Mon. Not. Roy. Astr. Soc.*, 341, 1157-1173.
- Terquem, C. E. J. M. L. J. (2008), New composite models of partially ionized protoplanetary disks, *Astrophys. J.*, 689, 532-538
- Thommes, E. W., and Lissauer, J. J. (2003) Resonant Inclination Excitation of Migrating Giant Planets. *Astrophys. J.*, 597, 566-580.
- Tsiganis, K., Gomes, R., Morbidelli, A., & Levison, H. F. (2005) Origin of the orbital architecture of the giant planets of the Solar System. *Nature*, 435, 459-461.
- de Val-Borro, M., et al. (2006) A comparative study of disc-planet interaction. *Mon. Not. Roy. Astr. Soc.*, 370, 529-558.
- Ward, W. R. (1991) Horeshoe Orbit Drag. *Lunar and Planetary Institute Conference Abstracts*, 22, 1463-1464.
- Ward, W. R. (1997) Protoplanet Migration by Nebula Tides. *Icarus*, 126, 261-281.
- Weidenschilling, S. J. (1977) Aerodynamics of solid bodies in the solar nebula. *Mon. Not. Roy. Astr. Soc.*, 180, 57-70.
- Wu, Y., and Murray, N. (2003) Planet Migration and Binary Companions: The Case of HD 80606b. *Astrophys. J.*, 589, 605-614.
- Yang, C. C., Mac Low, M.-M., and Menou, K. (2009) Planetesimal and Protoplanet Dynamics in a Turbulent Protoplanetary Disk: Ideal Unstratified Disks, *astro-ph*, arXiv:0907.1897v1.
- Yu, Q., and Tremaine, S. (2001) Resonant Capture by Inward-migrating Planets *Astron. J.*, 121, 1736-1740.

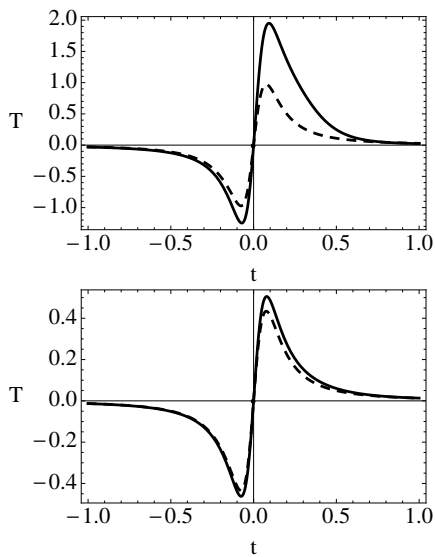


Fig. 5.— Torque on the particle of mass  $M$  that is normalized by  $10^3 M \Omega_p^2 a^2$  as a function of time in units of the planet’s orbit period along the unperturbed (dashed lines) and perturbed paths (solid lines). The planet mass  $M_p = 10^{-6} M_s$  (0.3 Earth masses for a planet that orbits a solar mass star). Top panel is for a particle having  $x = 0.02a$ , the case in Fig. 3. The bottom panel is for a particle with  $x = 0.03a$ .

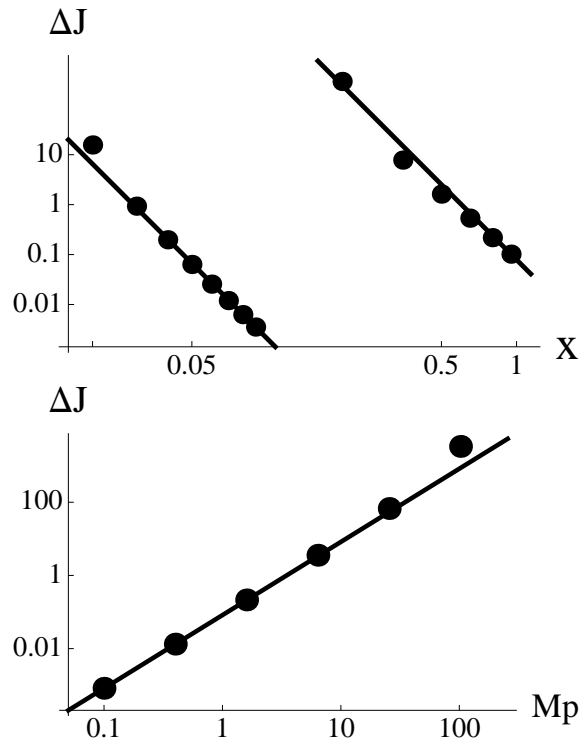


Fig. 6.— Numerical test of equation (8) based on orbit integrations. Top panel: Log-log plot of  $10^4 \Delta J / (M a^2 \Omega_p)$  as a function of preimpact distance from the planet’s orbit  $x$  in units of  $a$ . The lower set of points is for a planet of mass  $M_p = 10^{-6} M_s$  (0.3 Earth masses for a planet that orbits a solar mass star). The upper set is for  $M_p = 10^{-3} M_s$  (a Jupiter mass for a planet that orbits a solar mass star). The solid lines are for  $\Delta J \propto x^{-5}$  that pass through the respective right-most points. Bottom panel: Log-log plot of  $10^5 \Delta J / (M a^2 \Omega_p)$  as a function of planet mass in Earth masses for a planet that orbits a solar mass star. The points are the results of numerical simulations for a fixed value of  $x = 0.2a$ . The solid line is for  $\Delta J \propto (M_p / M_s)^2$  that passes through the left-most point.

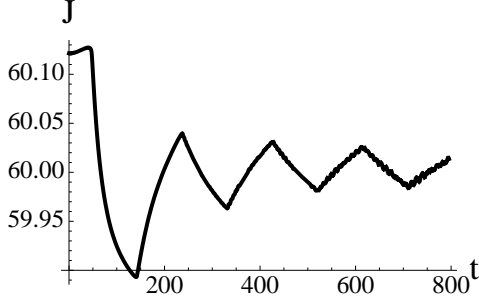


Fig. 7.— Total angular momentum for a set of 60 particles, each of mass  $M$ , on horseshoe orbits in units of  $Ma^2\Omega_p$  as a function of time in units of the planet orbit period in a star-planet system with  $M_p = 3 \times 10^{-6} M_s$  (0.3 Earth masses for a planet that orbits a solar mass star). The particles start at  $t = 0$  distributed between  $r = a + R_H/60$  to  $r = a + R_H$  (with  $R_H \simeq 7 \times 10^{-3} a$ ) along the star-planet axis 180 degrees from the planet. The changes in angular momentum cause a torque to be exerted on the planet. The torque (the time derivative of  $J$ ) oscillates and declines in time as angular momentum becomes more constant in time because the particles undergo phase mixing on the libration timescale  $\sim 150$  planet periods.

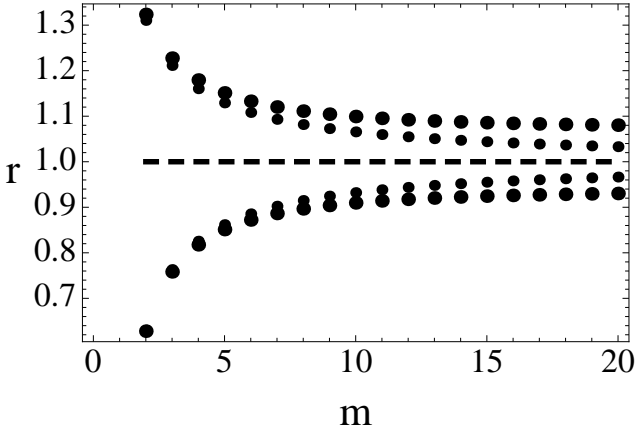


Fig. 8.— Radius of a Lindblad resonance in units of  $a$  as a function of azimuthal wave number  $m$ . Points below (above) the dashed line are for inner (outer) Lindblad resonances. The dashed line is the location of the planet. The two sets of smaller dots are for a Keplerian disk with radii given by equation (38). The resonances get closer to the planet with increasing  $m$ . The two sets of larger dots account for azimuthal pressure effects in a disk with thickness to radius ratio  $H/r = 0.1$ . With these pressure effects included, the resonances maintain a fixed separation from the planet at high  $m$ .

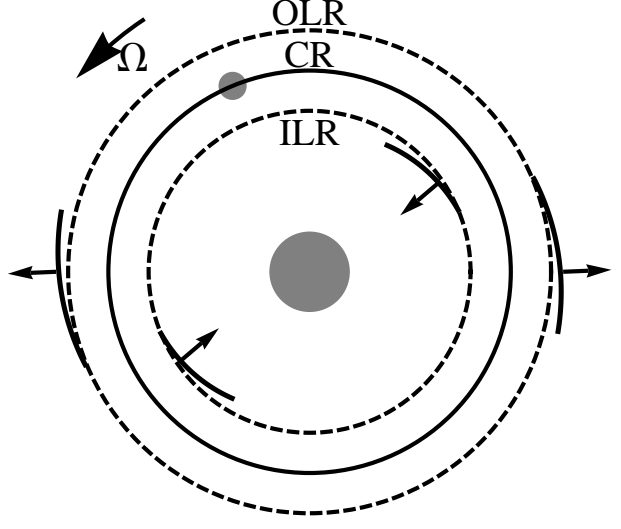


Fig. 9.— Schematic of acoustic (pressure) wave propagation in a gas disk involving an inner Lindblad resonance (ILR), outer Lindblad resonance (OLR), and corotation resonance (CR). Spiral waves launched at Lindblad resonances propagate away from the orbit of the planet. The region near the CR, between ILR and OLR, is evanescent (nonpropagating).

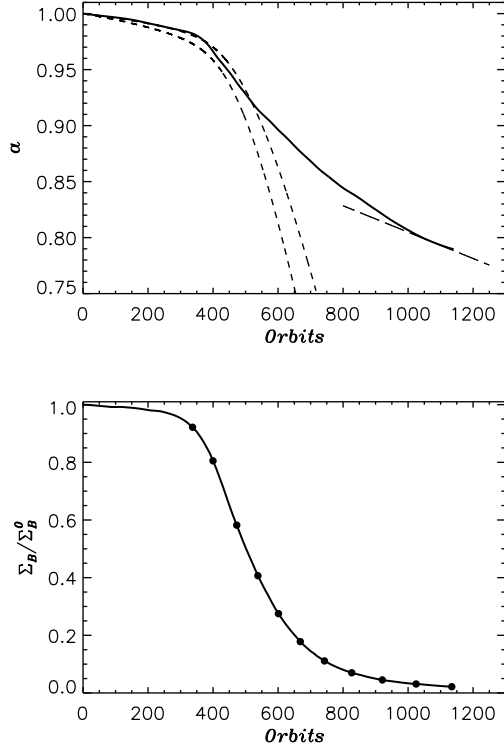


Fig. 10.— Migration of a planet orbiting a solar mass star and undergoing growth via gas accretion. The disk parameters are similar to those in Fig 1. Top: The vertical axis is the orbital radius in units of the initial orbital radius 5.2AU. The horizontal axis is time in units of the initial orbital period 12yr. The solid curve is the result of 3D hydrodynamical simulations. The lower and upper short dashed curves are based on equations (40) and (41) respectively, applied to a planet of variable mass. The long dashed curve corresponds to migration on the disk viscous timescale. Bottom: Average disk density near the planet relative to the initial value as a function of time. The density is averaged over a band of radial width  $2H$  centered on the orbit of the planet and is normalized by its initial value. The first solid circle marks the time when  $M_p = 16.7M_\oplus$ , subsequent circles occur at integer multiples of  $33M_\oplus$ . The planet initially follows the predictions of Type I migration theory in the top panel while there is no substantial gap in the disk (no drop in the curve on the bottom figure). After gap opening, the planet follows Type II migration. Obtained from *D'Angelo & Lubow, 2008*.

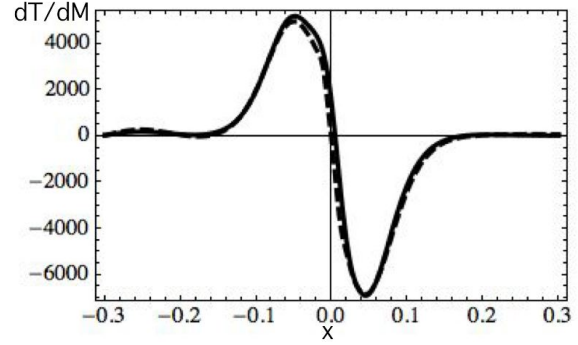


Fig. 11.— Scaled torque per unit disk mass on the planet as a function of radial distance from the planet's orbital radius based on 3D simulations. The horizontal scale is in units of  $a$  and the vertical scale is in units of  $GM_s(M_p/M_s)^2/a$ . The solid and long-dashed curves are for  $1M_\oplus$  (1 Earth mass) and  $10M_\oplus$  mass planets, respectively, that orbit a solar mass star. The disk parameters are  $H/r = 0.05$  and  $\alpha = 0.004$  for both the cases. According to linear theory, these two curves should overlap. Torque distributions are averaged over one orbital period. Figure based on *D'Angelo & Lubow, 2008*.

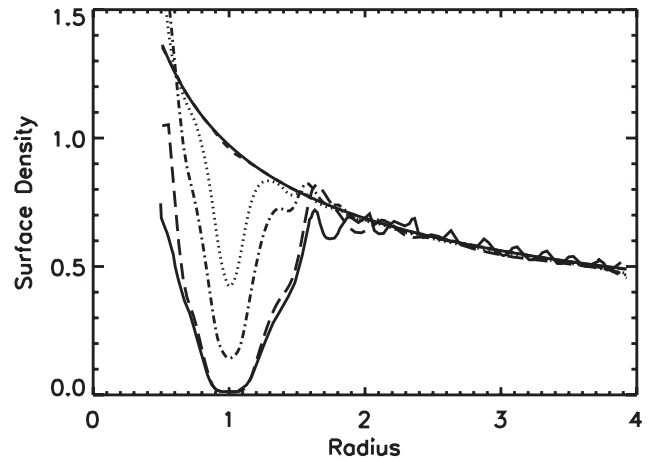


Fig. 12.— Azimuthally averaged disk surface density normalized by the unperturbed value at radius  $a$  as a function of  $r$  in units of  $a = 5.2AU$ . The central star has a solar mass. The disk is simulated in 3D with parameters  $H/r = 0.05$  and  $\alpha = 0.004$ . The density profiles are for planets with masses of 1 (long-dashed), 0.3 (dot-dashed), 0.1 (dotted), 0.03 (short-dashed), and 0.01 (thin solid)  $M_J$ . Only planets with masses  $M_p \gtrsim 0.1M_J$  produce significant perturbations. The thick solid line is based on a 2D simulation of a  $1M_J$  planet by Lubow et al (1999). Obtained from *Bate et al, 2003*.



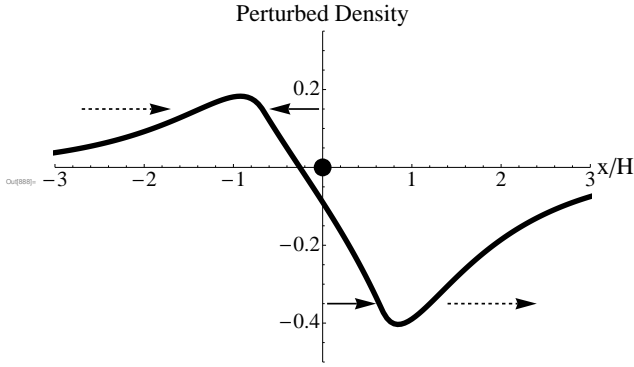


Fig. 13.— Schematic of the axisymmetric density perturbation in arbitrary units as a function of radial distance from the planet (shown as dot at the origin) in units of disk thickness  $H$ . The solid lines with arrows indicate the velocity perturbation on the gas caused by tidal torques on the planet. These velocities are directed away from the orbit of the planet. The dashed lines with arrows indicate the gas velocity, in the frame of the planet, due to the assumed inward migration of the planet. Interior to the orbit of the planet, the velocities due to tides and migration oppose each other and lead to a pile up of material. Outside the orbit of the planet, the velocities reinforce each other and lead to a density drop.

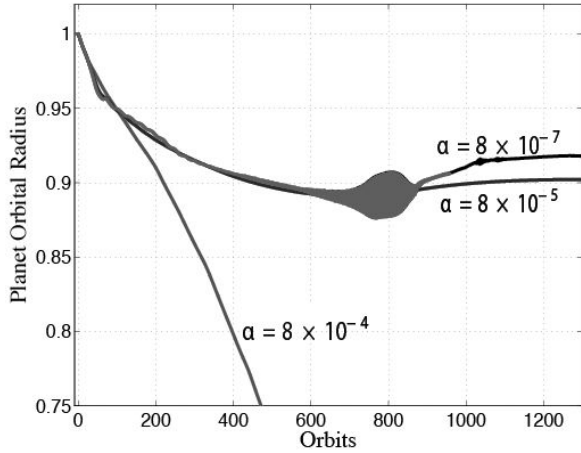


Fig. 14.— Influence of disk viscosity parameter  $\alpha$  on the migration of a planet with mass  $10M_{\oplus}$  in a disk with  $H/r = 0.035$  and mass  $\sim 0.1M_{\odot}$  based on 2D simulations. The vertical axis is the orbital radius in units of the initial orbital radius. The horizontal axis is the time in units of the initial planet orbital period. For  $\alpha = 8 \times 10^{-4}$  the migration follows the Type I rate. At the lower values, the migration halts due to a feedback effect (see Fig. 13). Figure based on *Li et al., 2008*.

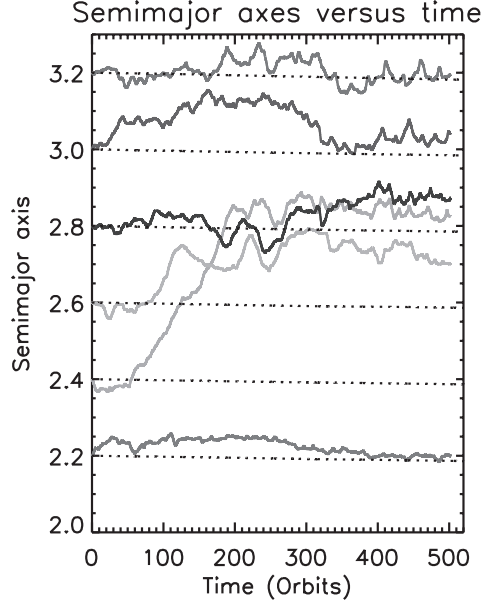


Fig. 15.— Orbital radius as a function of time in orbits for  $3M_{\oplus}$  planets embedded in a gaseous disk based on simulations. The dotted lines plot the migration of planets in a disk without turbulent fluctuations. The solid lines plot the migration of planets in a disk with turbulent fluctuations due to the MHD turbulence. The random motions are due to the fluctuating torques. Obtained from *Nelson, 2005*.

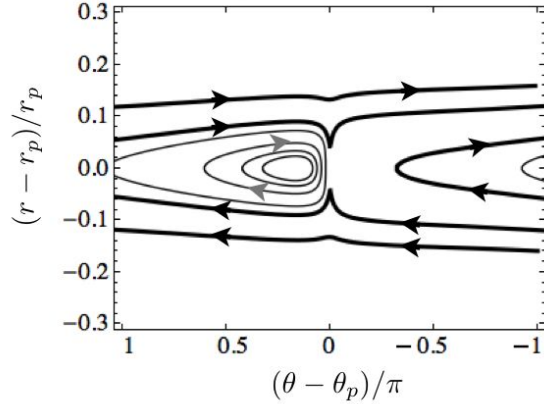


Fig. 16.— Coorbital streamlines near an inwardly migrating Saturn mass planet  $M_p = 3 \times 10^{-4}M_s$  located at the origin in the comoving frame of the planet that orbits a solar mass star. The inward migration rate is  $0.002\Omega_p a$ . Angle  $\theta$  increases to the left. The heavy streamlines are open and pass by the planet. The light streamlines are closed and contain trapped material on the leading side of the planet (streamlines based on *Ogilvie & Lubow, 2006*). The trapped material, acquired at earlier time, is retained from regions further from the star. The open streamlines carry ambient disk material. In contrast to the nonmigrating case in Fig. 2, the asymmetry and the density differences between the trapped (retained) and open (ambient) gas gives rise to a coorbital torque.

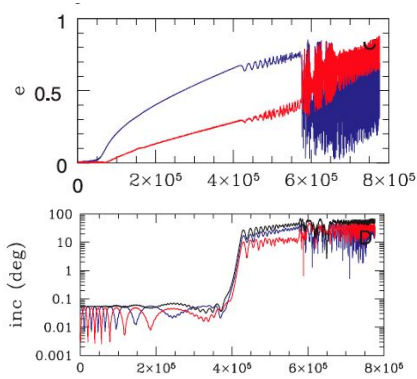


Fig. 17.— Evolution of orbital eccentricity (top) and inclination (bottom) of a two-planet system in which an inward migration of  $10^{-5} \text{AUyr}^{-1}$  is imposed on the outer one. The horizontal axis is in units of years. Both planets have a mass equal to Jupiter’s mass. The orbital eccentricities of the planets grow as a result of resonant migration in the 2:1 resonance. The eccentricity of the inner planet grows faster than the outer one. A small initial mutual inclination grows to large values as the eccentricities increase. From *Tommes & Lissauer, 2003*.

Out[879]=

